NASA/TM—2015-218832

Shape Memory Alloy Rock Splitters (SMARS)—A Non-Explosive Method for Fracturing Planetary Rocklike Materials and Minerals

Othmane Benafan and Ronald D. Noebe
Glenn Research Center, Cleveland, Ohio

Timothy J. Halsmer
Jacobs Technology, Cleveland, Ohio

July 2015

NASA STI Program . . . in Profile

Since its founding, NASA has been dedicated to the advancement of aeronautics and space science. The NASA Scientific and Technical Information (STI) Program plays a key part in helping NASA maintain this important role.

The NASA STI Program operates under the auspices of the Agency Chief Information Officer. It collects, organizes, provides for archiving, and disseminates NASA's STI. The NASA STI Program provides access to the NASA Technical Report Server—Registered (NTRS Reg) and NASA Technical Report Server—Public (NTRS) thus providing one of the largest collections of aeronautical and space science STI in the world. Results are published in both non-NASA channels and by NASA in the NASA STI Report Series, which includes the following report types:

- TECHNICAL PUBLICATION. Reports of completed research or a major significant phase of research that present the results of NASA programs and include extensive data or theoretical analysis. Includes compilations of significant scientific and technical data and information deemed to be of continuing reference value. NASA counter-part of peer-reviewed formal professional papers, but has less stringent limitations on manuscript length and extent of graphic presentations.

- TECHNICAL MEMORANDUM. Scientific and technical findings that are preliminary or of specialized interest, e.g., "quick-release" reports, working papers, and bibliographies that contain minimal annotation. Does not contain extensive analysis.

- CONTRACTOR REPORT. Scientific and technical findings by NASA-sponsored contractors and grantees.

- CONFERENCE PUBLICATION. Collected papers from scientific and technical conferences, symposia, seminars, or other meetings sponsored or co-sponsored by NASA.

- SPECIAL PUBLICATION. Scientific, technical, or historical information from NASA programs, projects, and missions, often concerned with subjects having substantial public interest.

- TECHNICAL TRANSLATION. English-language translations of foreign scientific and technical material pertinent to NASA's mission.

For more information about the NASA STI program, see the following:

- Access the NASA STI program home page at http://www.sti.nasa.gov

- E-mail your question to help@sti.nasa.gov

- Fax your question to the NASA STI Information Desk at 757-864-6500

- Telephone the NASA STI Information Desk at 757-864-9658

- Write to:
  NASA STI Program
  Mail Stop 148
  NASA Langley Research Center
  Hampton, VA 23681-2199

NASA/TM—2015-218832

Shape Memory Alloy Rock Splitters (SMARS)—A Non-Explosive Method for Fracturing Planetary Rocklike Materials and Minerals

Othmane Benafan and Ronald D. Noebe
Glenn Research Center, Cleveland, Ohio

Timothy J. Halsmer
Jacobs Technology, Cleveland, Ohio

National Aeronautics and
Space Administration

Glenn Research Center
Cleveland, Ohio 44135

July 2015

Acknowledgments

Funding from the NASA Space Technology Mission Directorate (STMD), Center Innovation Fund (CIF) is gratefully acknowledged. Manufacturing and imaging support from Grant E. Feichter, D.J. Brinkman, B.R. Caswell, and D. Brown are gratefully acknowledged. Material development support from (ARMD) Transformational Tools & Technologies (TTT) project is gratefully acknowledged. The authors thank S.A. Padula II, G.S. Bigelow, A. Garg, and D.J. Gaydosh, (shape memory alloy team) for helpful discussions. The authors also thank C.M. Creager and P.B. Abel for support in the SLOPE facility.

Level of Review: This material has been technically reviewed by technical management.

Available from

NASA STI Program
Mail Stop 148
NASA Langley Research Center
Hampton, VA 23681-2199

National Technical Information Service
5285 Port Royal Road
Springfield, VA 22161
703-605-6000

This report is available in electronic form at http://www.sti.nasa.gov/ and http://ntrs.nasa.gov/

Shape Memory Alloy Rock Splitters (SMARS)—A Non-Explosive Method for Fracturing Planetary Rocklike Materials and Minerals

Othmane Benafan and Ronald D. Noebe
National Aeronautics and Space Administration
Glenn Research Center
Cleveland, Ohio 44135

Timothy J. Halsmer
Jacobs Technology
Cleveland, Ohio 44135

Abstract

A static rock splitter device based on high-force, high-temperature shape memory alloys (HTSMAs) was developed for space related applications requiring controlled geologic excavation in planetary bodies such as the Moon, Mars, and near-Earth asteroids. The device, hereafter referred to as the shape memory alloy rock splitter (SMARS), consisted of active (expanding) elements made of $Ni_{50.3}Ti_{29.7}Hf_{20}$ (at.%) that generate extremely large forces in response to thermal input. The preshaping (training) of these elements was accomplished using isothermal, isobaric and cyclic training methods, which resulted in active components capable of generating stresses in excess of 1.5 GPa. The corresponding strains (or displacements) were also evaluated and were found to be 2 to 3 percent, essential to rock fracturing and/or splitting when placed in a borehole. SMARS performance was evaluated using a testbed consisting of a temperature controller, custom heaters and heater holders, and an enclosure for rock placement and breakage. The SMARS system was evaluated using various rock types including igneous rocks (e.g., basalt, quartz, granite) and sedimentary rocks (e.g., sandstone, limestone).

1.0 Introduction

Solar system exploration has been reliant on state-of-the-art space technologies ranging from navigation systems, to propulsion, to scientific instruments. These missions often include close contact with planetary bodies (e.g., the Moon, Mars, asteroids and comets) where in-situ environmental sampling is sought. In such cases, scientific instruments are built to detect, collect and characterize samples from the atmosphere, dust particles, soil, rock samples, or aeolian deposits amongst others. This provides researchers with geologic and climate history for a better understanding of near-Earth planets, asteroids and the evolution of the objects as a whole. However, certain areas of interest such as large rocks or hard craters are often not examined due to the site size, rock rigidity or inadequate capability of on-board tools for extraction of appropriate samples. This is mainly due to the restrictions in physical space and weight to carry necessary equipment to space, inability to use typical tools from the lack of gravitational forces, or for mission safety reasons (e.g., carrying explosives onboard spacecraft and rovers). Consequently, only surface sampling (e.g., through brushing), dust (e.g., through boring and drilling) or small, loose rocks can be examined. Moreover, based on revolutionary discoveries by previous space missions, it is of interest not only to analyze matter on the planetary bodies, but also to return soil and rock samples to Earth for more detailed studies and investigations. As a result, rock breaking capability onboard spacecraft can be enabling for the examination of internal structures or compositions of larger geologic structures, and if appropriate, transfer of relevant samples back to Earth for more rigorous studies.

Rock breaking and splitting is a common task on Earth, accomplished using many different methods. Dynamically, explosive (blasting) methods have frequently been used to break large rock formations in mines and drilling operations. Static methods have also been employed such as fluid pressure cells, chemical agents, and hydraulic wedges. Most of these methods, however, are not suitable for space applications due to the large size and weight of the equipment. Moreover, demolition techniques generate dust, noise, vibrations and flying debris that can interfere with space vehicle components (e.g., sensors, detectors, cameras) and pose safety concerns. Even in the case when static agents and pressure fluids are used, these methods are time-consuming, risk contamination of the environment, and do not guarantee chemical reactions with certain rocks, especially unknown rock structures on distant planets. As a result, there is a need for compact, reliable and cost-effective methods for static rock splitting.

One way of accomplishing this task is by taking advantage of shape changing materials known as shape memory alloys (SMAs). SMAs are materials that possess the unique ability to recover large deformations and generate high stresses in response to thermal or mechanical stimuli. This behavior occurs by virtue of a crystallographically reversible martensitic phase transformation between a high symmetry austenite phase and a low symmetry martensite phase. In general, when this type of material is deformed, the induced deformation can be recovered by applying heat above a certain threshold temperature referred to as the austenite start (A_s) temperature. On the other hand, when the material is deformed and constrained from recovering, it can generate extremely large forces upon the application of heat. This high power/weight ratio characteristic makes SMAs suitable for large force applications, such as static rock breaking.

SMAs for rock breaking concepts have been proposed in the past for ground-based applications. Nishida et al. (Refs. 1 to 4) have demonstrated the concept using conventional NiTi alloys where a maximum recovery force of 100 kN (566 MPa) was attained when the SMA elements was heated to approximately 90 °C with hot water. Carosio et al. (Refs. 5 and 6) have also used NiTi (A_s = 95 °C) and NiTiCu (A_s = 66 °C) alloys where stresses of about 800 and 650 MPa were obtained, respectively. Jing et al. (Refs. 7 to 9) have disclosed a method for directional fracture of rocks in which NiTi, iron-based, or copper-based shape memory alloys were used as the pressure transfer body. In this case, the rock breaker embodiment (i.e., the SMA shapes and placement) was similar to the work done by Nishida et al. (Ref. 1). An and Nam (Ref. 10) utilized ternary Ti-Ni-Cu alloys with compositions ranging from 5 to 20 at.% Cu with activation temperatures below 100 °C. This approach utilized the expansion stresses of the SMA rods along with additional plates for maximizing the load transfer. Lee (Ref. 11) developed a static rock crusher where the load transfer is accomplished by converting the vertical displacement of an expanding SMA into horizontal stress using wedge-shaped metals. Glushchenkov et al. (Ref. 12) developed a jaw breaker where the shape memory material is used for thrust rods and reset springs. Chevakin, et al. (Ref. 13) made a power actuator where the load-bearing casing of the actuator body is made of a material such as a NiTi alloy to reduce the space of the chamber, forcing the working medium to exert a force on the actuating member. Yamauchi and Sato (Ref. 14) used a Ti-Ni alloy consisting of 49.0 to 51.0 at.% Ni that was aged at 400 to 500 °C to produce a SMA rock crusher predeformed by compression at room temp and has thermal restoring function at ≥50 °C. Watabe (Ref. 15) developed a static crushing agent made of SMA pieces in conjunction with a hydrate inflating agent and an admixture of sand. The mixture is filled in a hole with water where expansion takes place once heated. In a more general conception, Coenen et al. (Ref. 16) have originated the idea of placing some expanding elements (such as an SMA) as part of a fracturing tool to exert a circumferentially varying pressure against the borehole wall. This notion was targeted for fracturing underground formations for the production of hydrocarbon fluids. Pelgrom (Ref. 17) has also considered a method for placing a body of shape memory metal within a tube targeted for subsurface formations for the production of hydrocarbons. Both of these concepts employ SMAs to generate a force on the borehole walls upon the application of heat. A comparison of these SMA-based methods and other techniques such as blasting for breaking rock can be found in Table 1 and Table 2, respectively.

TABLE 1.—COMPARISON OF ROCK SPLITTING METHODS AND APPLICATIONS BASED ON SHAPE MEMORY ALLOYS

	Methods	Principle of operation	Example applications	References
Non-Explosive Methods	Shape memory alloy rock splitter (SMARS)	NiTiHf high temperature shape memory alloy	Foreign planets (e.g., Mars), Martian volcanic rocks, asteroids, comets, proppants, spacers, fragile geological sampling, fossils, structure reinforcement, mining, oil drilling *A_s = 156 °C, **σ_{rec} = 1.5 GPa	Current work and 18
	Actuator for rock splitting	NiTi and NiTiCu actuators	Quarrying industry A_s = 95 °C, σ_{rec} = 0.8 GPa (NiTi) A_s = 66 °C, σ_{rec} = 0.65 GPa (NiTiCu)	5, 6, and 19
	Static rock breaker	TiNi-shaped memory alloy	Mining, civil and construction engineering A_s = 90 °C, σ_{rec} = .566 GPa	1 to 4
	Shape memory alloy Stone Breaker	NiTi, Fe-based, Cu-based	Stone exploitation, tunnels, side slopes, presplitting blasting and demolition blasting	7 to 9
	Static stone breaker using ternary SMA	Ti-Ni-Cu alloy (5 to 20 at.% Cu)	Stoner breaker A_s < 100 °C	10
	Stress transfer device	Wedge-type static rock crusher using SMAs	Rocks	11
	Apparatus for breaking monolithic objects	Jaw breaker using shape memory material for thrust rods and reset springs and liners for recovery	Monolithic objects	12
	Power actuator	Load-bearing casing of the actuator body are made of a “form remembering” material such as a NiTi alloy	Mining and construction for working rock quarries, fracturing of oil reservoirs and gas-bearing strata, presses, jacks, guillotines	13
	Method and tool for fracturing an underground formation	Placement of elements (such as an SMA) to exert a circumferentially varying pressure against the borehole wall.	Production of hydrocarbon fluids, oil and gas production,	16
	Method for placing a body of shape memory metal within a tube	SMAs generate a force on the borehole walls upon the application of heat	Subsurface formation for the production of hydrocarbons	17
	Shape memory alloy for rock crusher	Ti-Ni alloy consisting of 49.0 to 51.0 at.% Ni aged at 400 to 500 °C	rock crushing Thermal restoring function at ≥50°C	14
	Rock crushing method	Shape memory alloy rods and heaters	Rock crushing, reduction of noise and oscillation	20
	Static Crushing Agent	A crushing agent made of a SMA formation piece with a hydrate inflating agent and an admixture of sand	Holes Restoring temperature of 50 to 100 °C	15

*A_s: Austenite start temperature, **σ_{rec}: Recovery stress

TABLE 2.—COMPARISON OF ROCK SPLITTING METHODS AND APPLICATIONS THAT DO *NOT* INVOLVE SHAPE MEMORY ALLOYS

	Methods	Principle of operation	Example applications	References
Non-Explosive Methods	Heat source	Heaters placed in a series of drilled small holes; the heat transmitted to the rock causes splitting	Splitting of granite, marble, and other rocks	21
	Thermal expansion	Metal reinforcement bars within concrete slabs are heated to cause thermal expansion for cracking	Ferroconcrete bodies, concrete	22
	Thermal expansion	Attaching and heating of two metals with dissimilar coefficient of expansion to cause distortion for splitting	Splitting of stone, either in quarrying or on a smaller scale	23
	Ripping	Large teeth attached to the back of a bulldozer/tractor	Populated areas, soft to moderately firm rocks	24
	Foam Injection	High-pressure foam	Rock excavation or secondary breakage (mining and tunneling)	25
	Flame jet	Ultra hot hydrogen flame (~4000 °C)	Mining industry	26 and 27
	Water injection	Hydraulic	Mining industry	28
	Plasma blasting	Copper-oxide/aluminum thermite reaction initiated by an electrical charge	Mining industry	29
	Cardox tube	High pressure gas (carbon dioxide)	Rock and concrete breakage, deep sea excavation, tunneling and shaft sinking and trenching and excavation	30
	Nonex	High pressure gas (propellant burning)	Slate mines, mine shafts,	31
	Penetrating Cone Fracture (PCF)	High pressure gas (propellant burning)	Mines, clearing of block grizzlies, crushers or chute (oversize)	30
	Pneumatic Fracturing	Gas (typically air or nitrogen)	Mining industry	32
	Thermal (cryogenic) fracturing	Thermal stresses from fluids colder/hotter than the reservoir	Mining industry	32
	Chemicals	Chemical reaction/pressure	Rock trenching, granite boulder breaking, rock removal, concrete demolition	32
Explosive Methods	Explosive blasting	Explosive charges	Canals, Watercourses, harbors, quarries, rock fracturing, dams, construction sites	33
	Presplitting	Create a secondary fracture plane before production blasting (light to heavy charges)	Competent, hard to extremely hard rock	34
	Trim (cushion) blasting	Light charges placed in single row of holes along the excavation line	Contoured slopes with benches or other slope variations	35
	Contour (smooth) blasting	Decoupled charges fired simultaneously in closely spaced holes	Mining industry	36

All of the abovementioned applications and concepts utilized SMAs, but to the best of the authors' knowledge, all of the SMAs incorporated in these devices exhibited activation temperatures below 100 °C and generated stresses of ≤800 MPa through isothermal (compressive or tensile) loading. When dealing with space applications, however, the harsh space environment poses added constraints and requirements for the design of space mechanisms. Constraints such as weight, size, operational temperatures, and ease of operation amongst others have always been of prime importance. SMARS, designed as part of this work is capable of activation at temperatures above 100 °C and generating nearly twice the stress of these other systems. It is also ideal for use in planetary rock drilling/sampling operations, where flying debris from blasting methods can destroy the rock formation of interest, pose safety concerns to the astronauts,

or cause damage to the costly nearby equipment (e.g., rover mirrors and sensors). In addition, static SMARS requires little setup and activation time compared to other static methods such as chemical agents that can take up to a few days to react with some hard and unknown rock formations. Mission reliability is another benefiting factor since SMARS operates based on a material response and only requires heat input to activate without the need for complex valve systems or hydraulic fluids, making it extremely simple and essentially fool proof to operate. The small volume and extremely low weight of the SMARS reduces payload launch costs and transportation hazards when compared to heavy hydraulic wedges and dangerous explosive materials and chemicals.

Thus, the goal of this work was to explore high-force, high-temperature SMAs, referred to as HTSMAs, for use as a static rock breaker where higher activation temperatures and greater force generation can be achieved. The SMARS device described herein employs Ni-rich NiTiHf alloys, which have shown promising results regarding actuation and stability (Ref. 37), as the expanding members. Along with custom heaters and transportable controller, SMARS key components and performance parameters were evaluated during trials using several rock types. In addition, new material conditioning methods were developed and optimized for prestraining the shape memory elements, which are simple enough that they could also be utilized in space to reset the actuators.

2.0 Principle of SMARS Operation

SMARS is a static rock breaking device developed with the objective to provide controllable rock splitting without any demolition damage to the sample or surrounding environment, compared to the alternative dynamic explosive or blasting approaches. It consists of (*i*) an expanding element made of NiTiHf alloys, (*ii*) a heating system that fits over the HTSMA member, (*iii*) end-tips used to contact the rock surface consisting of various end geometries (i.e., conical, spherical, cylindrical, helical or flat ends), and (*iv*) a temperature controller and thermocouples for device process operation (Figure 1).

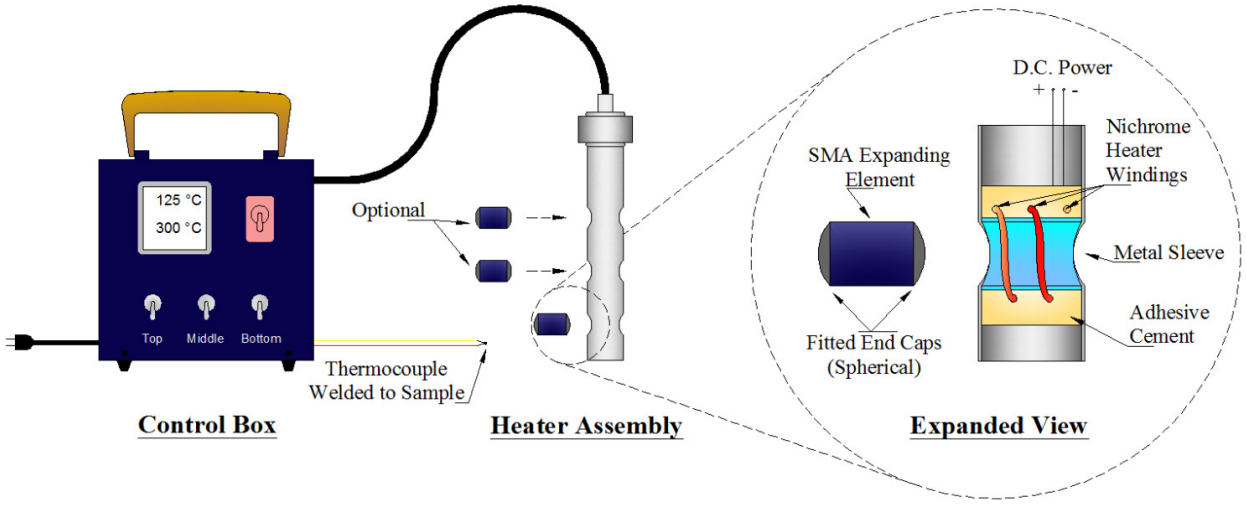

Figure 1.—SMARS components showing a schematic of the control box, the heater assembly and an expanded view of the heater internal construction and SMA placement.

SMA conditioning: The actuator material (i.e., the NiTiHf alloy) in the form of a cylindrical pellet is initially conditioned, henceforth referred to as "*training"*, to produce desirable forces once activated. The training methods used are described in the forthcoming sections. After training, the material exists in the low temperature martensite phase where the end-conditions are mechanically attached or directly machined on the trained material. The effective length from tip to tip is made equal to a predrilled borehole diameter for proper operation (Figure 2(c)).

Heaters and SMARS placement: Custom heaters, made of Nichrome wires and stainless steel housing, are placed over the trained HTSMAs and inserted into a predrilled borehole in the area of interest within a rock or pre-existing cracks (Figure 2(d)). Multiple assemblies can be placed within the rock to magnify the force or provide additional displacement necessary for complete rock splitting, especially of larger samples.

SMARS activation: The final step is to deliver a power signal to the heaters using a DC power supply or other power source to activate the device. On heating, the trained material undergoes a phase transformation to the high temperature austenite phase, where in the unconstrained condition a shape recovery would normally occur (i.e., expansion in this case). However, since the device is confined by the borehole wall, the SMA cannot initially expand; instead it exerts a force at the contact area resulting in rock fracture (Figure 2(e)). After the rock splitting, the device can be recovered and reused for successive employments, given that a new SMA piece will be used, or the same SMA member can be retrained.

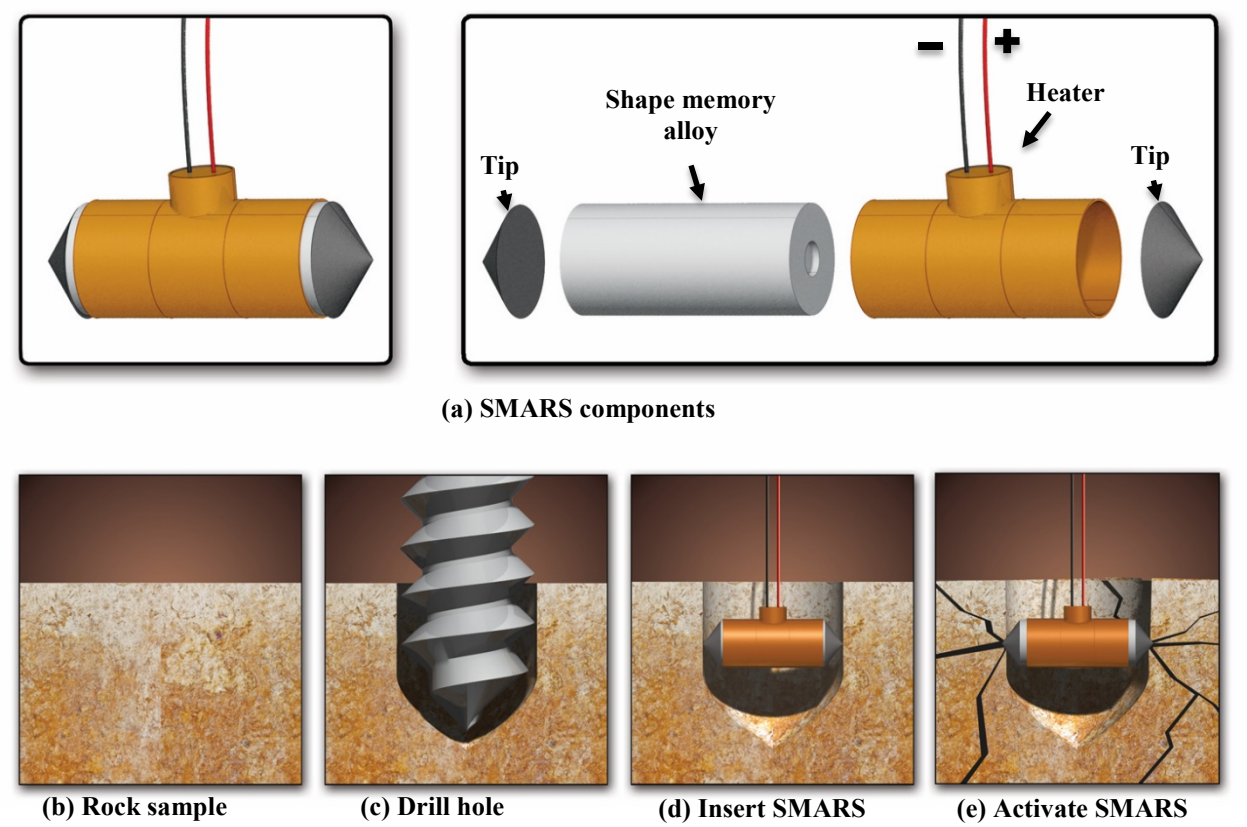

Figure 2.—Principle of SMARS operation: (a) assembled and exploded view of SMARS components. (b) Rock sample before drilling. (c) Hole drilling corresponding to the SMA length. (d) SMARS placement within the borehole. (e) SMARS activation after heating to above the austenite finish (A_f) temperature.

3.0 Materials and Procedures

3.1 Material

The material used in this work was a ternary Ni-rich $Ni_{50.3}Ti_{29.7}Hf_{20}$ (at.%) alloy produced by vacuum induction melting. The casting was vacuum homogenized at 1050 °C for 72 h, followed by extrusion at 900 °C through an area reduction ratio of ~7:1. SMARS pellets and other test specimens were machined from the extruded rods (Ext. 189) and subjected to an aging treatment of 3 h at 550 °C followed by furnace cooling. Various physical and thermomechanical properties of heat-treated alloys of similar composition are available in the literature (Refs. 37 and 37).

3.2 Thermomechanical Testing and Training

Thermomechanical testing was conducted using a servohydraulic load frame equipped with a high-temperature extensometer and an Ameritherm (Ambrell) induction heating system. Prior to any testing, each specimen was gripped on the frame and subjected to two stress-free (<1 MPa) thermal cycles between 30 and 300 °C to relieve any residual stresses resulting from the sample machining and handling. The transformation temperatures: martensite start (M_s), martensite finish (M_f), austenite start (A_s), and austenite finish (A_f) were determined from the stress-free, strain-temperature response and were 141, 126, 156, and 170 ± 2 °C, respectively.

In order to achieve the anticipated forces and displacements necessary for effective SMARS operation, several training processes were used. Training is a process used to produce a desirable shape memory/superelastic response by performing selected mechanical, thermal and/or thermomechanical loading procedures. Training is typically performed to stabilize the cyclic response of an SMA and reduce dimensional instability (Refs. 39 and 40), to shape set a specific form (Ref. 41), or to introduce a particular behavior such as the two-way shape memory effect (TWSME) (Ref. 42). In the case of SMARS, training was used to attain the highest possible blocking forces (i.e., the forces generated during the constrained heating, also known as recovery forces) with the highest possible displacements. For this purpose, two different training methods were investigated, referred to as isothermal and isobaric training routines.

Isothermal training: This method consisted of deforming the material in the martensite phase at room temperature to a specific strain (or stress) level. The resulting blocking stresses were determined by holding the strain constant (before unloading) while thermal cycling between 30 and 300 °C.

Isobaric training: In this method, the material was thermomechanically cycled twice under a constant stress between 30 and 300 °C. To measure the blocking force generated by this technique, the material was unloaded to zero stress at the end of the second isobaric thermal cycle, the remnant strain was held constant and the constrained sample was again thermally cycled between the temperature limits of 30 and 300 °C.

Repeated isothermal training and evaluation cycles were used to verify the ability to reuse/retrain NiTiHf elements for SMARS operation. During this process, the material was deformed in the martensite phase at room temperature to a specific stress value, followed by unloading to zero stress. At this point, the blocking force was measured by holding the remnant strain constant while cycling between 30 and 300 °C. This procedure was repeated again multiple times, i.e., loading and unloading followed by constant strain thermal cycling, to determine the viability of the alloy to be used in repeated SMARS applications.

TABLE 3.—MECHANICAL AND PHYSICAL PROPERTIES OF SELECTED ROCK MATERIALS
DATA PRESENTED IN THIS TABLE WAS OBTAINED FROM REFERENCES 32 AND 33

Properties	Igneous rocks			Sedimentary rocks	
	Basalt	Granite	Quartz	Sandstone	Limestone
Density, g/cm^3	2.8 to 3.0	2.6 to 2.7	2.6 to 2.8	2.2 to 2.8	2.3 to 2.7
Uniaxial compressive strength, MPa	341	250	300	170	250
Tensile strength, MPa	10	7 to 25	5 to 20	4 to 25	6 to 25
Elastic modulus, GPa	40 to 80	30 to 70	150 to 300	15 to 50	20 to 70
Strain at failure, %	0.35	0.25	0.2	0.2	----------
Fracture mode I toughness	0.11 to 0.41	>0.41	>0.41	0.027 to 0.041	0.027 to 0.041
Porosity, %	0.22 to 22.1	1.02 to 2.87	0.40 to 0.65	1.62 to 26.4	0.27 to 4.10
Drilling rate index, DRI	20 to 75	30 to 80	25 to 80	15 to 90	30 to 100
Hardness, Vickers	450 to 750	725 to 925	1060	550 to 1060	125 to 350

3.3 Rock Selection and Properties

Several categories of rocks were used for the assessment of the SMARS performance. The rock selection was made based on the types that are typical to lunar and Martian igneous and sedimentary deposits, and other forms that can be found in solar system planets, asteroids or comets. The igneous rocks used were basalt and granite. Sandstone and limestone were used as examples of sedimentary type rocks. Basic properties of these rocks can be found in Table 3. Cylindrical-shaped boreholes were drilled in each rock sample using diamond core drill bits with an outer diameter of 19.05 mm (0.75 in.).

4.0 Prototype Hardware Design

End-tips: In addition to the HTSMA used as the expanding member, several other components were indispensable to the design of SMARS. One of these components is the end-tips. The end-tips directly attach to the HTSMA member and were designed for two purposes: first was the interchangeability of tips depending on the rock types or hardness, and second was to compensate for any gaps between SMARS and the rock surface in the case of an irregularly shaped borehole. Several end-tips were designed including conical, spherical, cylindrical, and flat ends (Figure 3). The flat ends were the simplest form and were designed for plane borehole walls or pre-existing cracks in the vicinity of the rock of interest. The conical ends were considered for acute penetration into the rocks to help with the crack initiation and ultimately propagation to fracture. Both the spherical and cylindrical ends were designed for maximizing the contact surface area within the borehole. In these cases, the end tip forms were machined to match the borehole diameter. Once the SMARS is used, presetting the form was achieved using custom platens that matched each of the end-tips (in the case of fixed tips). In the current study, a servohydraulic frame was used to apply resetting loads, but a hand pump equipped with a heater can also be used if resetting is required on remote sites.

Pushers: Due to the limited strain recovery of most SMAs (approximately 2 to 5 percent strain), the strains (or displacements) produced are occasionally insufficient for complete rock splitting, particularly for small boreholes. Nonetheless, it is noted that a complete splitting is not necessarily the goal in all cases. Often, only initial cracking is desired near wells or other critical areas such as fragile fossils. When complete splitting is required, SMA pushers were designed to provide additional displacement after the main HTSMA members have been activated. The pushers were made in the form of helical springs

(Figure 4) with axial spring rates ranging from 175 to 875 N/mm (1000 to 5000 lbf/in) with displacement exceeding 10 percent from the solid height (fully compressed). The pushers are placed in the top position of the heater assembly shown in Figure 1, and are heated sequentially after the bottom and/or middle HTSMA members are fully expanded. As a result, these pushers are not required to provide high blocking forces, but provide additional displacements to fully split the rock.

Heaters: Three types of heating systems were considered for SMARS operation. The heater design shown in Figure 1 was custom made using a metallic sleeve, adhesive cement, and Nichrome wires housed in the heater assembly. This design was compact in size and capable of heating to very high temperatures (exceeding 400 °C) in a relatively short period of time (seconds to 1 min). The second design consisted of using commercial flexible Kapton (DuPont) or Thermofoil (Minco Products, Inc.) heaters that are wrapped around and bonded to the HTSMA members. Although this was the lightest and least power-consuming heating method (10 W/in^2), it was very time consuming and in some cases the desired temperatures were not reached due to the small surface area of the HTSMA members in contact with the heaters. The final method consisted of using induction heating. This technique is preferred for large, dry boreholes. Induction heating yields the fastest heating rates, but requires much higher power consumption (e.g., 120 V AC) and footprint (a separate power supply is needed to power the induction unit).

Controller: SMARS operation was controlled using a custom-built controller box comprised of a 0 to 20 mA temperature indicator with retransmission, a 24 V DC power supply, selector switches to trigger the individual heaters either simultaneously or sequentially, connectivity for type-K thermocouples, and a main power switch to activate the chosen heaters. A circuit diagram of the controller components is shown in Figure 5.

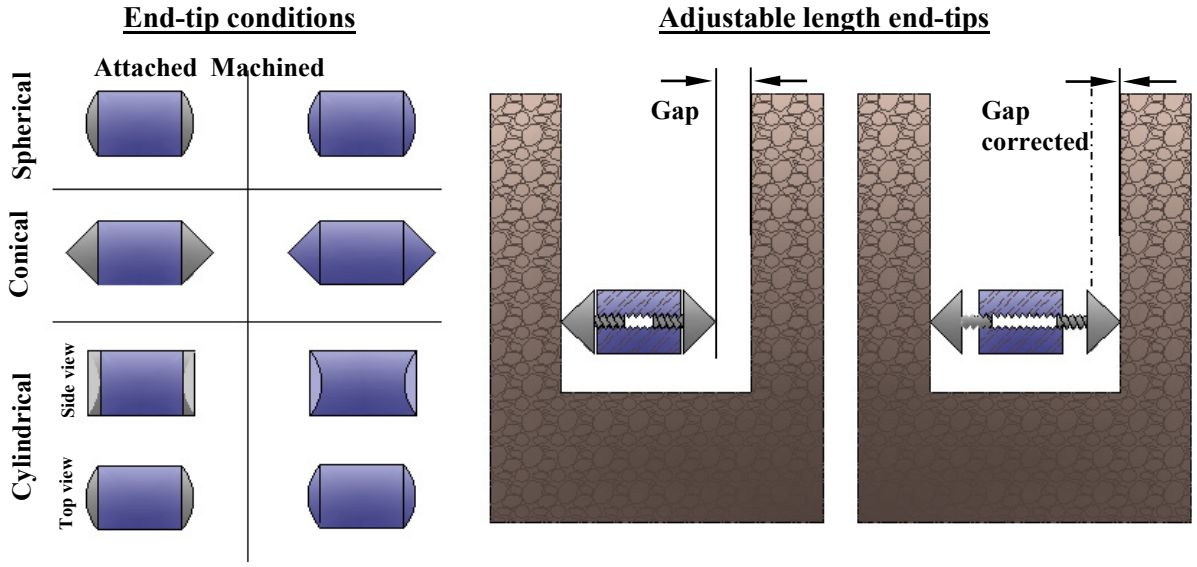

Figure 3.—End-tip conditions and method for gap adjustment.

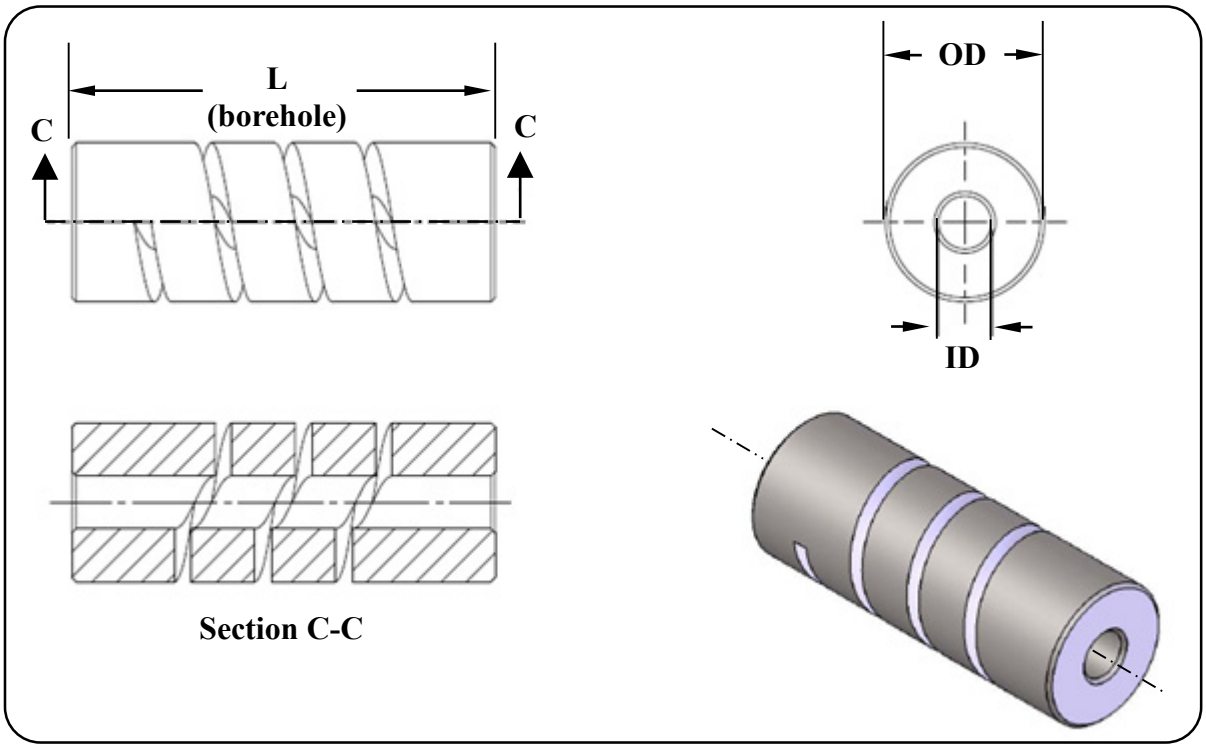

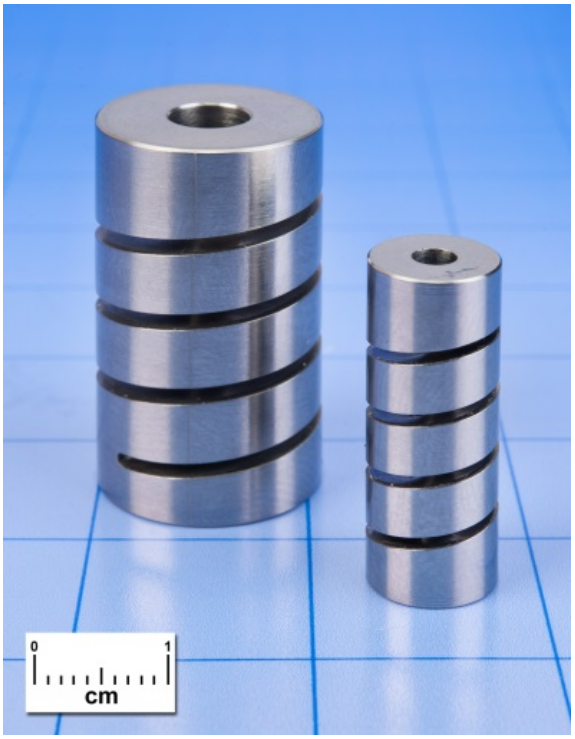

Figure 4.—Shape memory alloy helical pushers. End-tips can also be attached to this component.

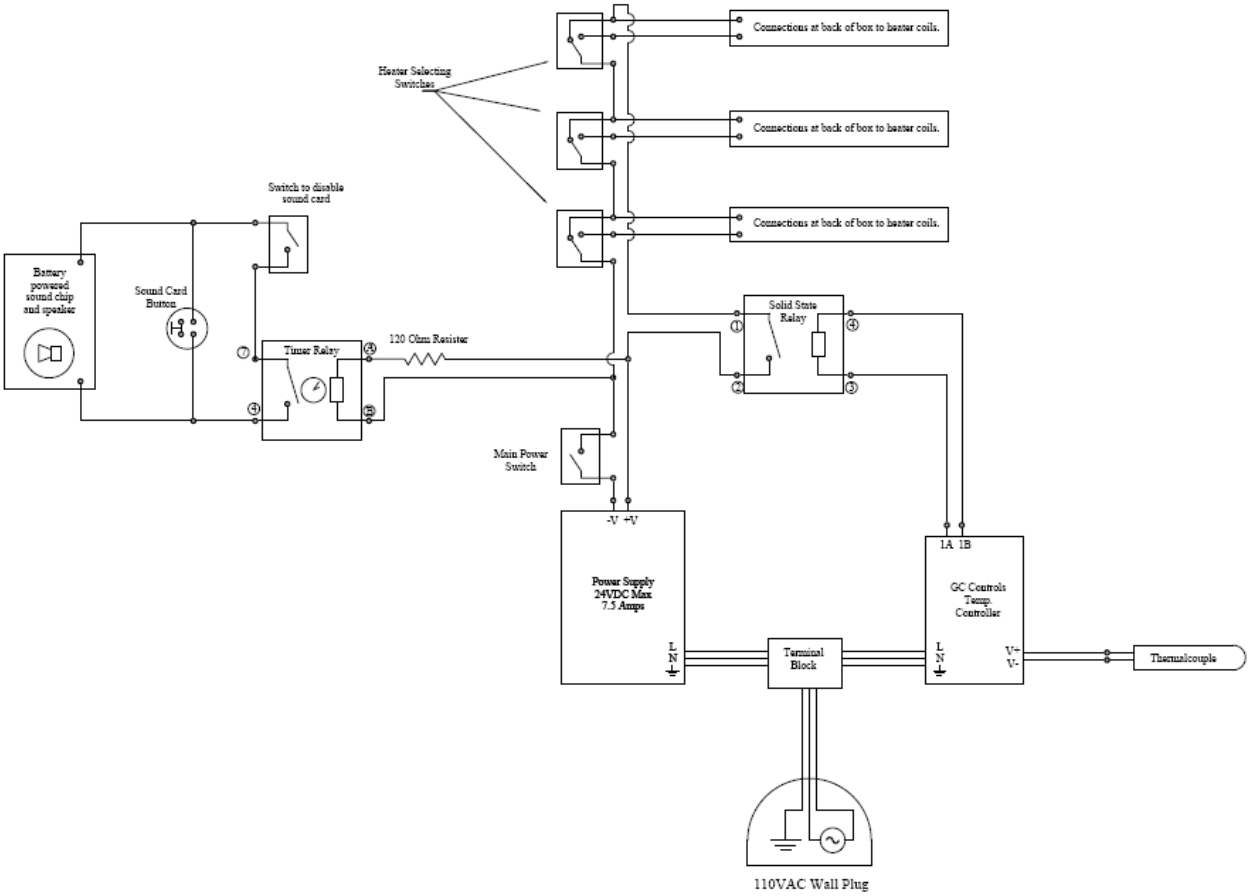

Figure 5.—Simplified controller circuit diagram.

5.0 Training Results and Discussions

5.1 Isothermal Training

The isothermal stress-strain response of the $Ni_{50.3}Ti_{29.7}Hf_{20}$ alloy in uniaxial compression at room temperature is shown in Figure 6. In addition to the reference load-unload cycle to –1000 MPa (solid line), individual samples were compressed to the indicated strain levels (open symbols) at which point the strain was held constant followed by thermal cycling. It was shown in previous studies that no plastic deformation attributed to slip was observed during the initial loading to –1 GPa (Ref. 37), however an increasing amount of inelastic deformation due to martensite variant reorientation/detwinning occurs with increasing stress (Ref. 37).

To determine the effect of this training procedure on the blocking stress, once the strain imposed at room temperature was held constant, each specimen was thermomechanically cycled twice between room temperature and 300 °C as shown in Figure 7. Note that two sample geometries were used for this purpose. The data presented in Figure 7(a) to (d) was produced from threaded, dogbone specimens 5.08 mm (0.2 in.) in diameter and 15.24 mm (0.5 in.) in gauge length. For these tests, it was possible to

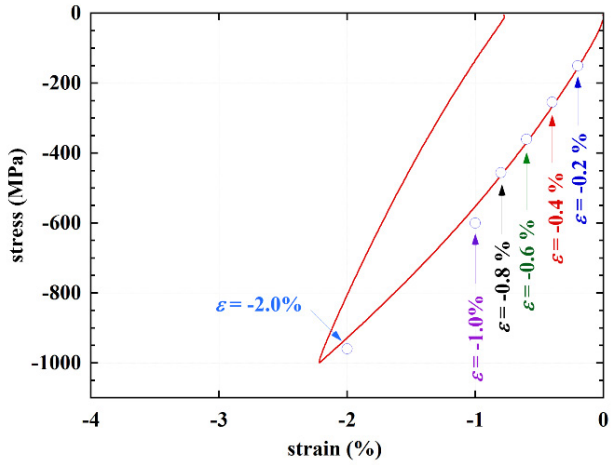

Figure 6.—Compressive stress-strain response of the $Ni_{50.3}Ti_{29.7}Hf_{20}$ alloy deformed at room temperature. The open symbols indicate the prestrain level imposed for each specimen (isothermal training) prior to temperature cycling shown in Figure 7.

allow the load to reverse to slightly positive values during thermal cycling as indicated by the dashed lines. For higher strains where buckling may become an issue with this sample geometry, compression samples 5 mm in diameter and 10 mm long were used to produce the data in Figure 7(e) and (f). In this case however, it was not possible to allow the load to reverse above the zero load line with the compression setup used. As a result, the lower cycle limit for temperature cycling was increased from 30 to ~50 °C resulting in a slightly compressive load (≤ –10 lbf) at the lower end of the thermal cycle in order to always maintain contact with the platens (Figure 7(e)).

In either geometry, the data exhibited similar trends. During the initial heating cycle, the material exhibited a transient behavior at around 150 to 170 °C where the stress went up briefly followed by a sharp decrease to a minimum value at the upper cycle temperature (300 °C). This behavior is only observed on the first cycle and it occurs at approximately the same temperature regardless of the applied strain. The second (and all succeeding cycles—not shown) exhibited typical hysteresis loops identified by the four characteristic temperatures. Because of the transient behavior during the initial cycle, the four transformation temperatures corresponding to the 2nd cycle are summarized in Figure 8. It is noted that accurate determination of the A_f temperatures was rather challenging due to the non-linear nature of the curves. Both the A_s and M_f transition temperatures, as determined by the intercept method, are shown to slightly decrease with increasing level of the applied strain imposed during thermal cycling. On the other hand, the A_f and M_s transition temperatures shifted to higher values as a function of applied strain.

The important feature relevant to the SMARS device is the magnitude of the stresses that can be generated after the trained and subsequently constrained sample is heated (Figure 7). The initial thermal cycle, in particular, simulates the operation of the SMARS device after isothermal training. In addition to the phase transformation, the material's thermal expansion also contributes to the maximum stress generation, which is prevalent in the linear region after the A_f temperature. It has also been found in previous studies (Ref. 43) and other unpublished work, that even after the apparent A_f temperature, there could be remnant martensite that continues to transform with increasing temperature. Nonetheless, both the continued phase transformation and the thermal expansion favor the stress generation in samples constrained in compression. However, the thermal expansion works against samples constrained in tension resulting in relaxation of the stress (Ref. 43).

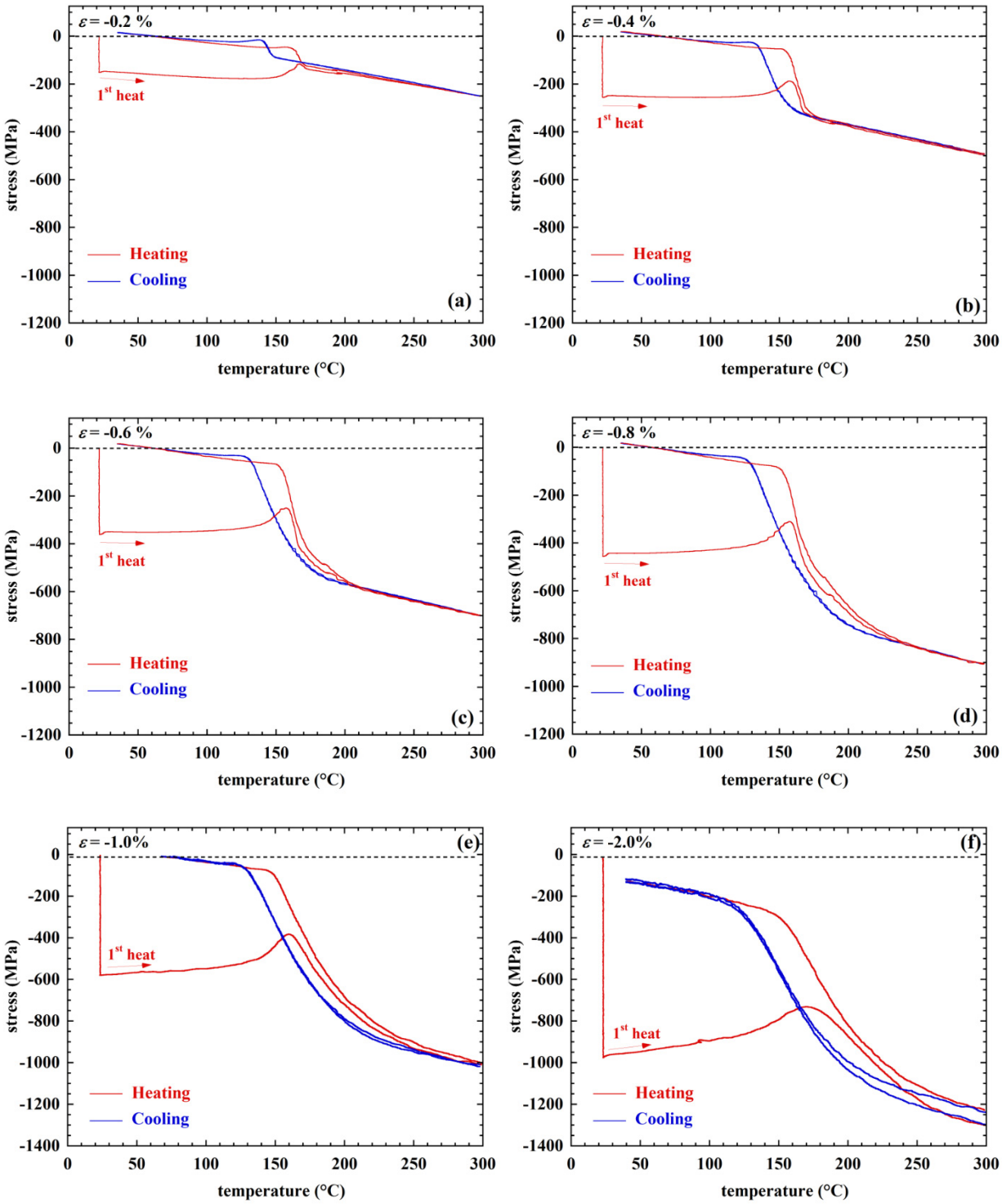

Figure 7.—Stress–temperature responses of the $Ni_{50.3}Ti_{29.7}Hf_{20}$ alloy corresponding to the isothermal training of Figure 6.

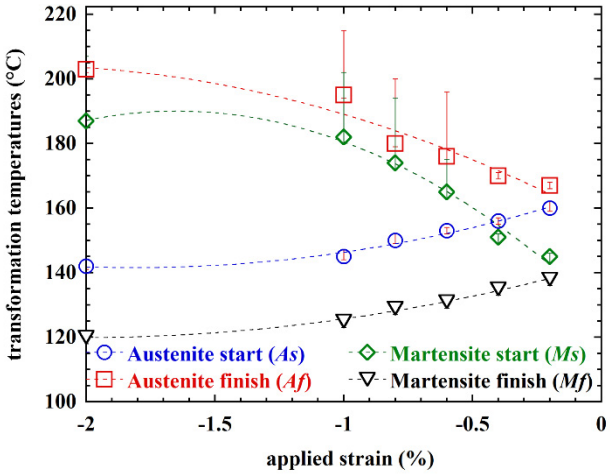

Figure 8.—Transformation temperatures determined from the 2nd cycle during the constant-strain, thermal cycling conditions.

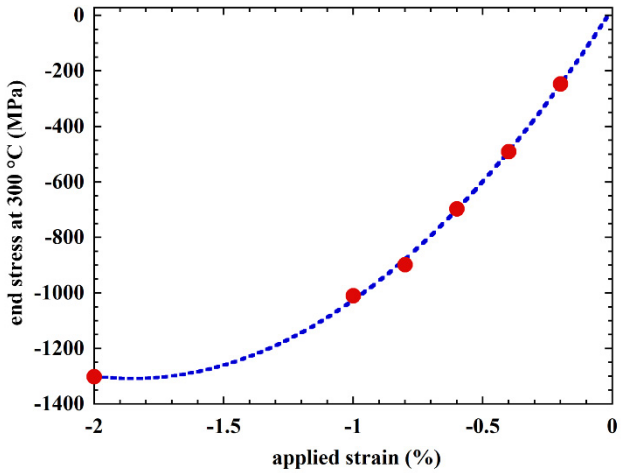

Figure 9.—End stresses measured in the austenite phase at 300 °C after the isothermal training as a function of the applied strain.

The maximum stresses generated, measured at the upper cycle temperature of 300 °C, are plotted as a function of applied strain level in Figure 9. For extended cycles (not shown), a decrease in blocking stress with cycling was evident for applied strains higher than –0.8 percent. This is largely due to yielding of the austenite phase once critical stresses are reached resulting in permanent plastic deformation as shown by Coughlin et al. (Ref. 44) and Benafan et al. (Ref. 37). However, only the first thermal cycle is pertinent to SMARS operation, and the largest stress is always generated during the first cycle. The maximum blocking stresses achieved through this training method was –1.3 GPa using an applied strain of –2 percent.

5.2 Isobaric Training

The strain–temperature response of the $Ni_{50.3}Ti_{29.7}Hf_{20}$ alloy in uniaxial compression is shown in Figure 10. Each specimen was thermomechanically cycled under a constant stress of –100, –200, –300 or –400 MPa, for two complete cycles. As opposed to the isothermal training method where the martensite was textured isothermally through mechanical loading at room temperature, in this isobaric training routine the martensite is preferentially textured via the initial loading and most predominantly through thermomechanical cycling under the constant stress. For example, under a constant stress of –200 MPa (Figure 10(b)), the initial loading resulted in ~0.35 percent strain, while a complete thermal cycle reduced the size of the sample by an additional 1.55 percent strain. Note that since this alloy is dimensionally stable, one single cycle is sufficient to reorient the martensite phase, as the two cycles overlap except for the initial heating cycle. But for examination purposes, two cycles were conducted in each trial. At the end of the second cycle, the material was unloaded to zero stress.

To determine the level of blocking stress developed by this training technique, the sample was fixed in strain at its new shape and the sample thermally cycled under constant strain. The corresponding blocking stress results are shown in Figure 11. Since the martensite is mostly oriented as part of this training method, the typical transient response as observed during isothermal training (Figure 7), did not occur. In this condition, blocking stresses built up on the first heating cycle followed by a stress relaxation close to zero upon cooling. Similar to the isothermal training, the nature of the transformation temperatures is analogous to the previous results.

The blocking stresses obtained in this training process were higher compared to the isothermal training method. Yet, the stress levels used in the isobaric training process (Figure 10) were much lower than the conjugate stresses attained during the prestrain (training) cycle, shown in Figure 6. For instance, isobaric training at –400 MPa (Figure 11(c)) resulted in a blocking stress of –1.5 GPa. On the other hand, a prestrain to –2 percent strain (conjugate stress of –2 GPa (Figure 6)) resulted in blocking stress of –1.3 GPa on the first cycle. Consequently, isobaric training is a more effective method for reorienting the microstructure for optimum blocking stress generation.

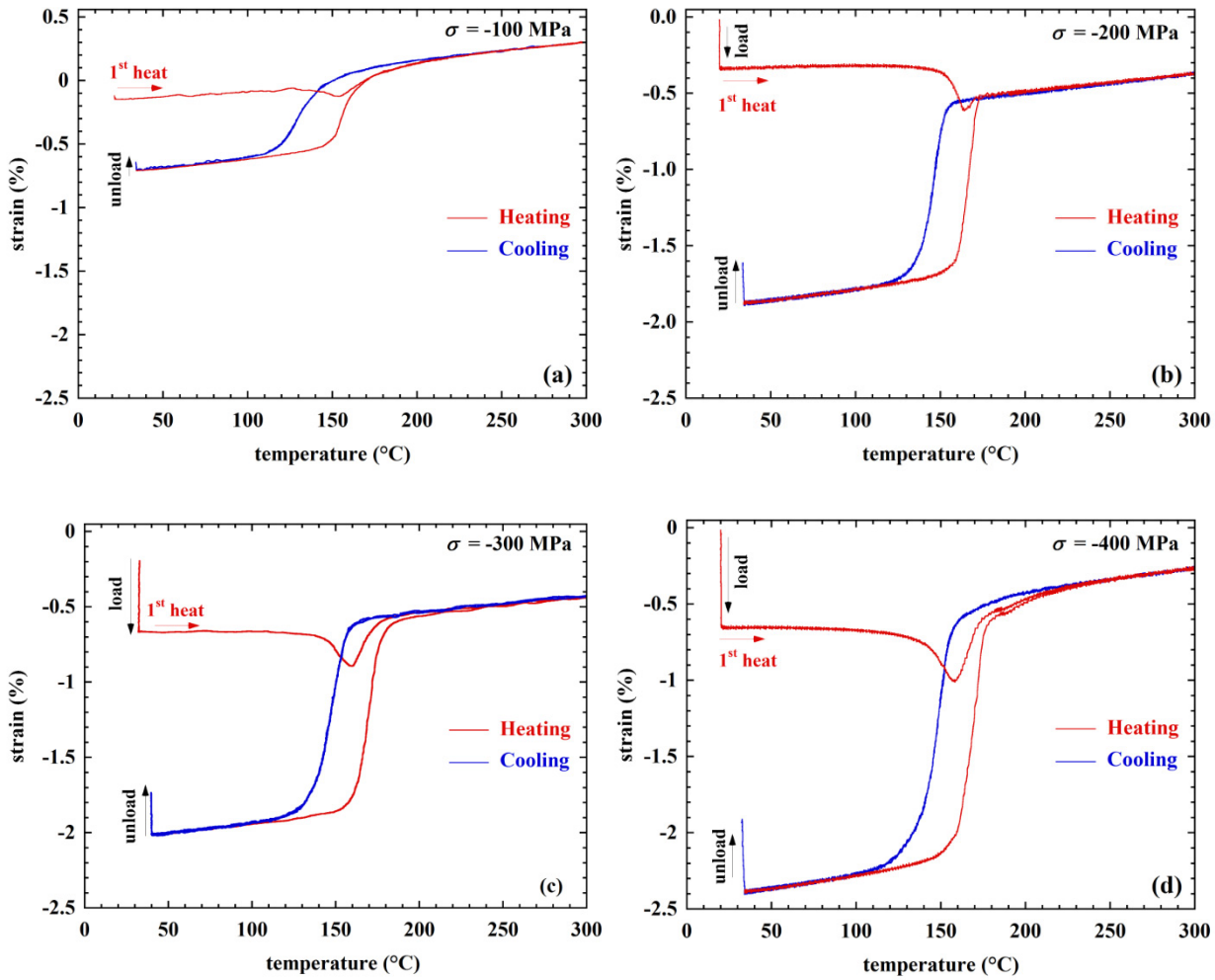

Figure 10.—Constant stress, strain-temperature response of the $Ni_{50.3}Ti_{29.7}Hf_{20}$ for the indicated stress level (isobaric training).

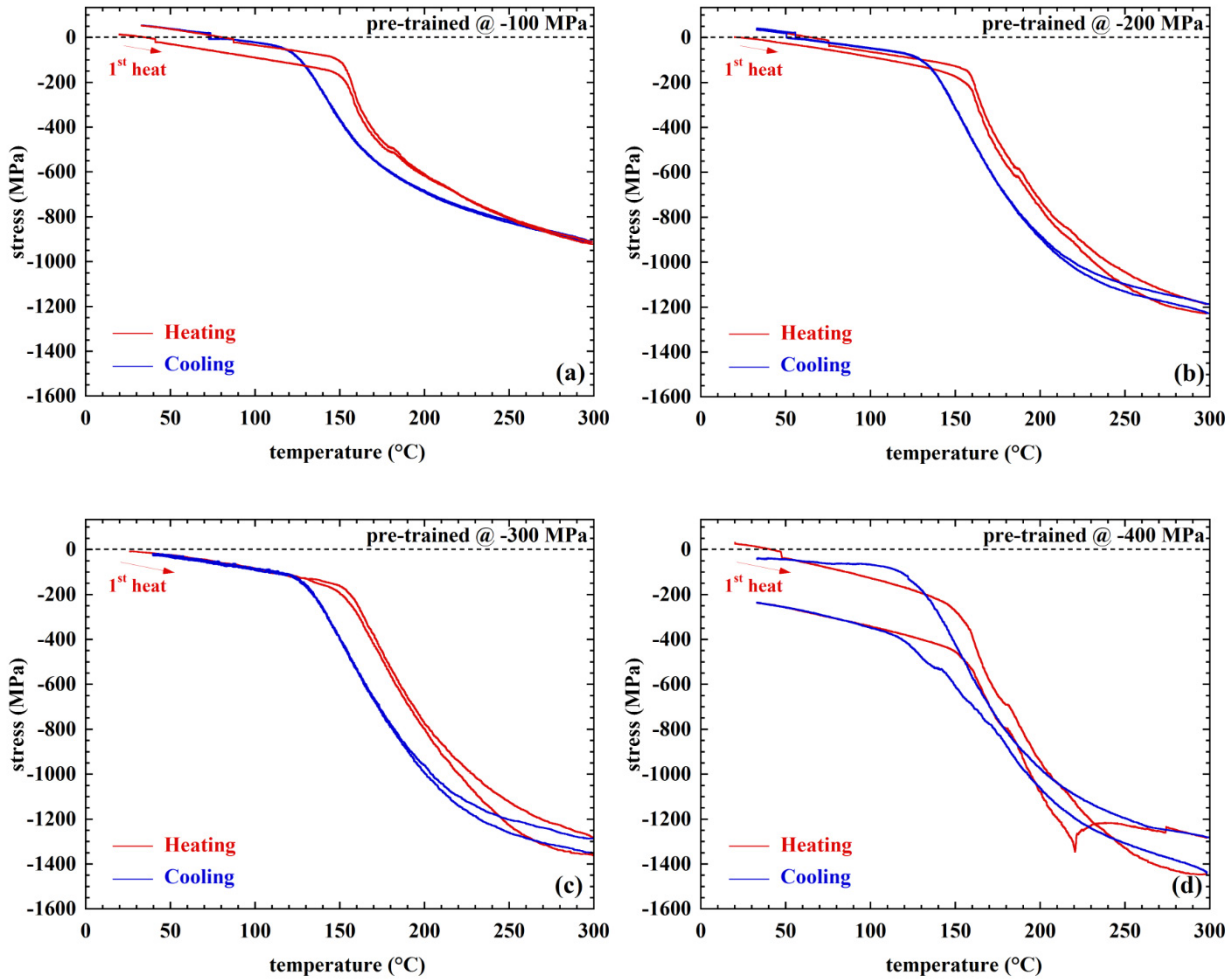

Figure 11.—Stress–temperature responses of the $Ni_{50.3}Ti_{29.7}Hf_{20}$ alloy corresponding to the isobaric training of Figure 10. The blocking stresses are generated during constant strain, thermal cycling after different training levels indicated in each plot.

A summary of the blocking stresses measured at 300 °C is shown in Figure 12. It may even be possible to obtain higher blocking stresses using this training method by additional martensite reorientation. The –400 MPa isobaric thermomechanical cycle yielded a transformation strain of –2.4 percent (Figure 10(d)), but it is known from previous work (Ref. 37) that additional transformation strain is possible with higher applied stresses. However, the load limit for the mechanical test setup was reached and could not accommodate much larger blocking stresses. Regardless, a significant improvement in blocking stress generation was achieved using this isobaric training process in comparison with the previous isothermal method. A blocking stress of nearly –1.5 GPa was attained by this technique, with a training stress of only –400 MPa.

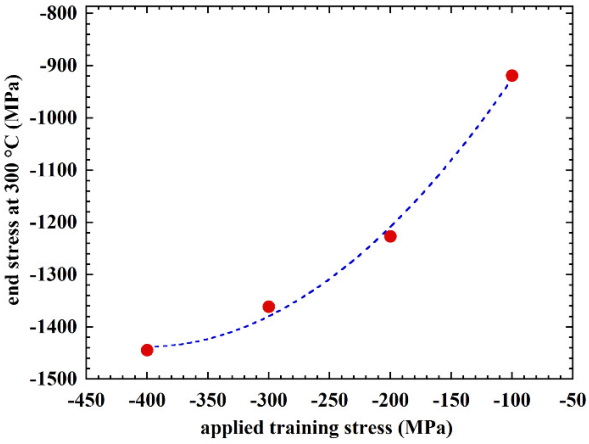

Figure 12.—End stresses measured in the austenite phase at 300 °C after the isobaric training as a function of the applied training stress.

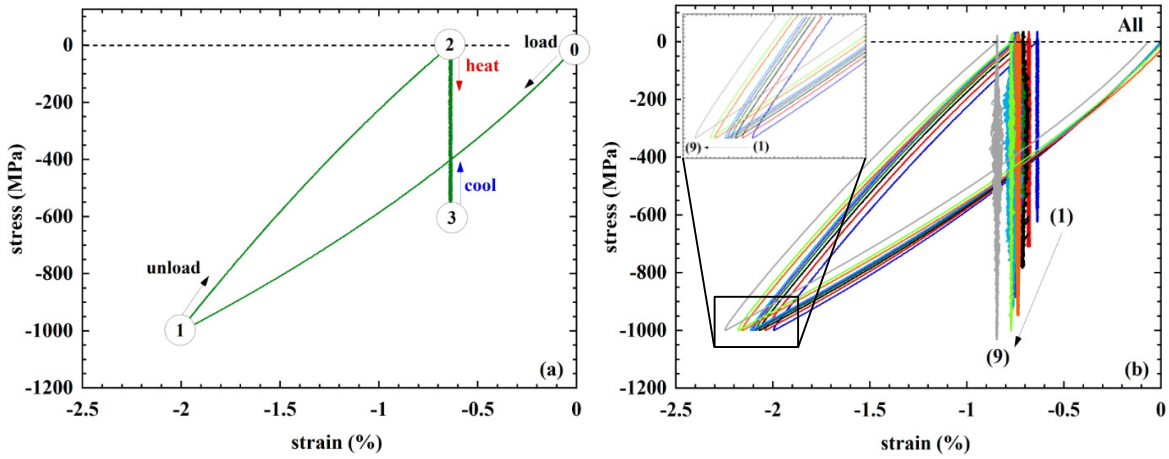

Figure 13.—Compressive stress-strain response of the $Ni_{50.3}Ti_{29.7}Hf_{20}$ alloy deformed to -1 GPa at room temperature. (a) The cyclic testing sequence, and (b) the 9 sequences showing the change with cycling.

5.3 Ability to Reuse/Retrain $Ni_{50.3}Ti_{29.7}Hf_{20}$ SMA Elements for SMARS Operation

Cyclic operation of the $Ni_{50.3}Ti_{29.7}Hf_{20}$ alloy was investigated to determine the effect of retraining on the behavior of the SMARS elements. During this process, the material was loaded, similar to the isothermal training routine except to a target stress instead of target strain level, to –1 GPa followed by unloading to zero stress. The remnant strain of approximately –0.8 percent was held constant while thermal cycling between 30 and 300 °C (Figure 13(a)). After the constant-strain cycling, the specimen was thermally cycled twice under 0 MPa, and the procedure was repeated. The stress-strain curves corresponding to each sequence (a sequence is defined by isothermal loading and unloading, constant-strain thermal cycles, and finally two stress-free thermal cycles) are shown in Figure 13(b). There is an apparent softening as shown by the inset, which is associated with an increase in blocking stresses (labeled 1 to 9). The stress-temperature responses corresponding to each of these sequences are shown in Figure 14. To better follow the trend, the data was plotted all together in the middle of Figure 14, while the individual responses are shown for sequences 1 to 8 labeled on the upper right corner of each plot. It is clearly shown that the blocking stresses gradually increase reaching approximately –1 GPa at the end of the 9th sequence (summarized in Figure 15). This additional increment in blocking stress is indicative of further martensite reorientation after each sequence.

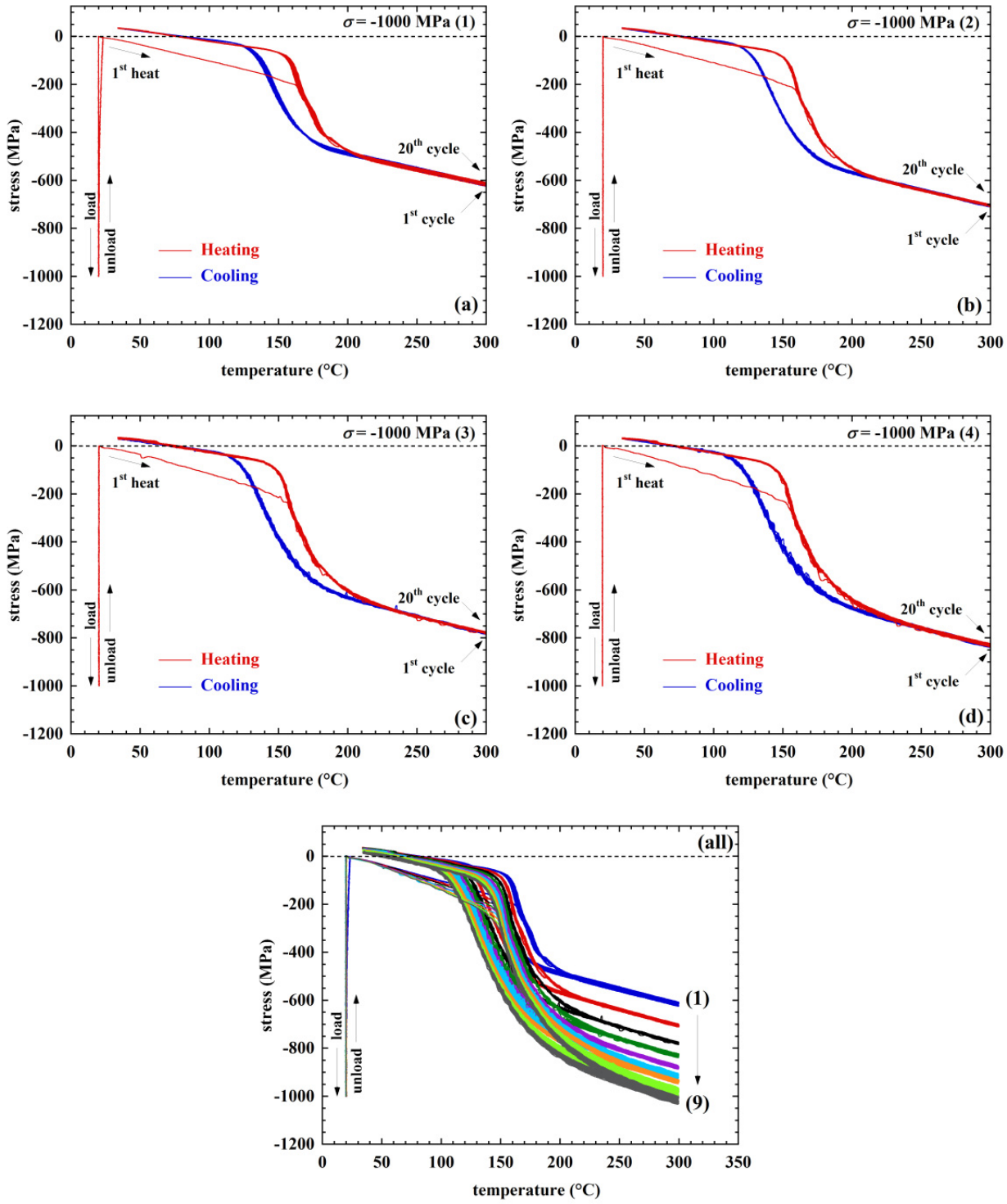

Figure 14.—Stress–temperature responses of the $Ni_{50.3}Ti_{29.7}Hf_{20}$ alloy corresponding to the cycling of Figure 13. For comparison purposes, all the responses were plotted together in the middle figure, while the individual responses are shown for sequences 1 to 8 labeled on the upper left corner of each plot.

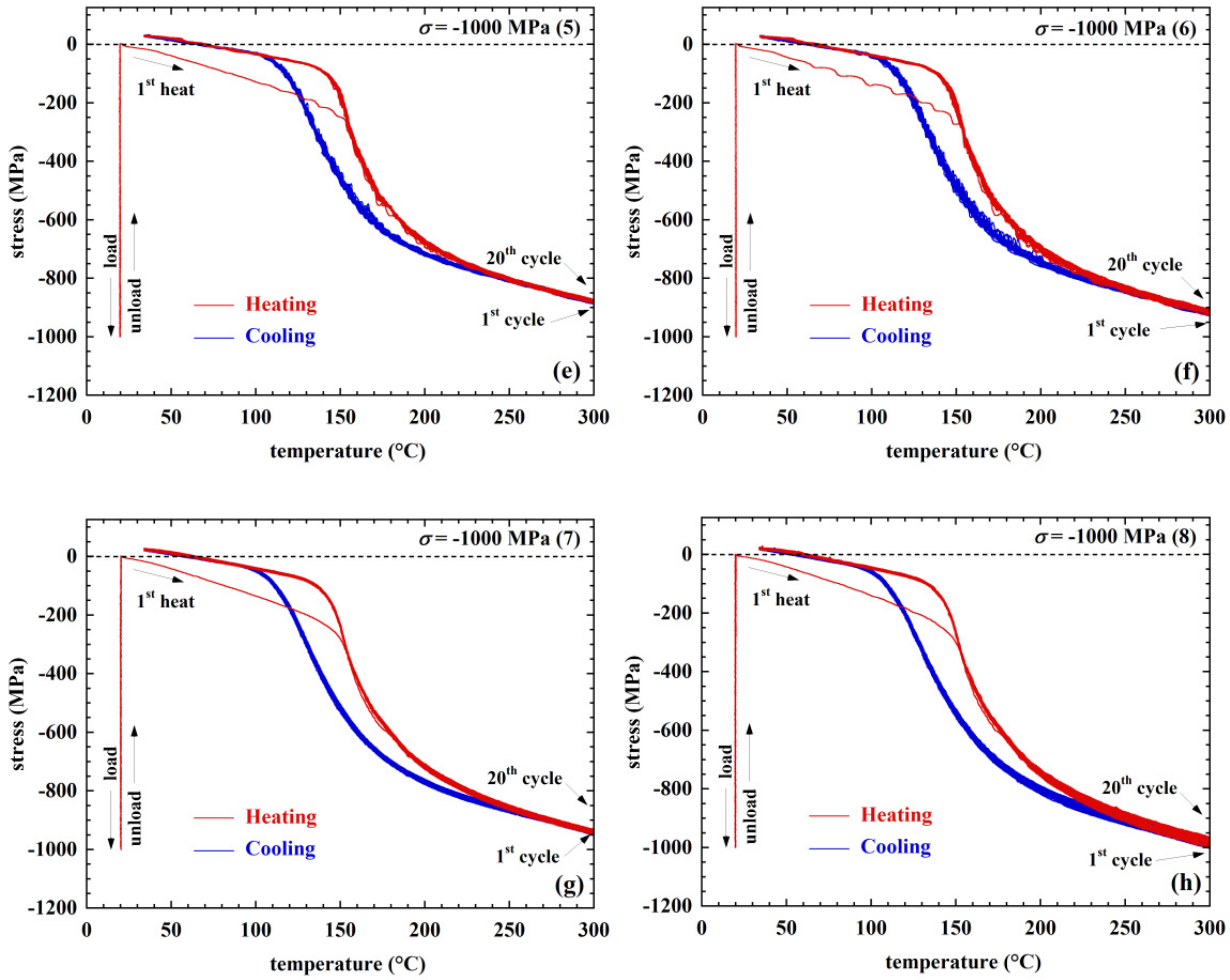

Figure 14.—Concluded.

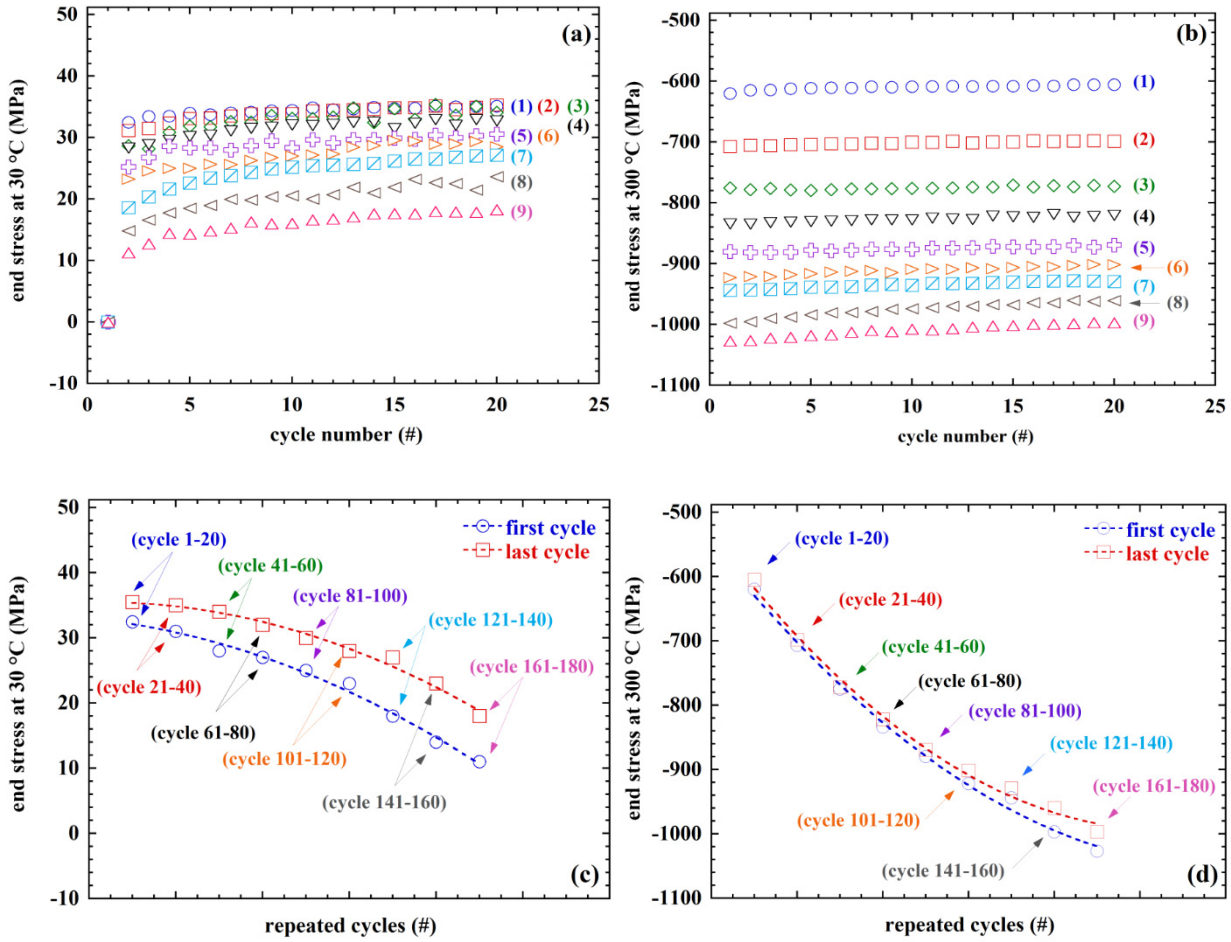

Figure 15.—End stresses measured in (a) and(c) the martensite phase at 30 °C and (b) and(d) the austenite phase at 300 °C. The data is plotted as a function of cycle number in (a) and (b), and as a function of the testing sequences in (c) and (d).

This behavior is further examined by considering the stress-free thermal cycles performed at the end of each sequence. The post strain-temperature behavior for each case is shown in Figure 16 where the data was combined in the middle of the figure, and the individual responses are shown for sequences 1 to 8 labeled on the upper left corner of each plot. Initially, the remnant strains are recovered and the no-load response is typical of that observed for as-extruded material with the strain change due to the uniaxial response of the volume change due to the martensitic transformation (Ref. 37) (Figure 16(a)). With repeated reloading and cycling, it is apparent that the random variant structure is being replaced by a structure consisting of compressive martensite variants resulting in a typical compressive strain-temperature response even without application of an external load (Figure 16(h)). This progression takes place by way of interplay between martensite variant reorientation and formation of lattice defects that aid the process, both of which are experimentally demonstrated by the generation of additional blocking stresses and the slight accumulation of residual strain, respectively.

Regardless of the microstructural mechanisms, it is noted that the cyclic operation of the $Ni_{50.3}Ti_{29.7}Hf_{20}$ elements actually resulted in an increase in blocking stresses and an improvement in performance. This actually demonstrates the benefit of retraining of the SMAs after use in SMARS and the advantages of the NiTiHf alloy used in this work.

6.0 SMARS Trials

The SMARS concept was evaluated using a custom testbed as shown in Figure 17(a). Predrilled rocks were positioned in an enclosure along with the supporting hardware as discussed previously. A variety of SMAs with different end-conditions were also fabricated as shown in Figure 17(b). Depending on the nature of the rock and desired outcome (i.e., cracking, or complete splitting), appropriate SMA elements (SMA plus end-tips) were placed within the heater assembly, which was then inserted in the drilled hole for testing. Over 35 trials were conducted on four rock types (basalt, granite, sandstone and limestone). The results, cracking and/or complete fracture of the rock samples are documented in Figure 18 to Figure 23.

In Figure 18, a $Ni_{50.3}Ti_{29.7}Hf_{20}$ sample, trained using the isobaric method under –200 MPa, was used to break a basalt rock. In this test, one SMA sample was placed 2.5 in. deep inside the borehole, with a thermocouple attached to the surface. Although cracking noises were audible at around 170 °C, the first visible crack was observed at approximately 198 °C. After that, the cracking continued until the SMA element was fully expanded at about 289 °C. The entire test from SMARS activation to full cracking took less than 1 min. Because of thermocouple placement the actual temperature of the SMA was lower but tracked that of the thermocouple.

Another basalt test was attempted using a binary $Ni_{49.9}Ti_{50.1}$ alloy element isobarically trained under –300 MPa (Figure 19). Previous attempts using isothermal training on binary NiTi were unsuccessful and did not result in any cracking. However, the isobaric training technique was proven to be more efficient (Secs. 5.1 to 5.2), and when utilized in this test resulted in full fracture of the basalt sample in just 38 sec. But it should be noted that the maximum blocking stresses obtained in this material were only 700 MPa as opposed to 1.5 GPa in the $Ni_{50.3}Ti_{29.7}Hf_{20}$ alloy. This means that less material can be used in the case of the $Ni_{50.3}Ti_{29.7}Hf_{20}$ alloy or higher stresses can be generated to break much larger specimens, which is typically an advantage for space missions.

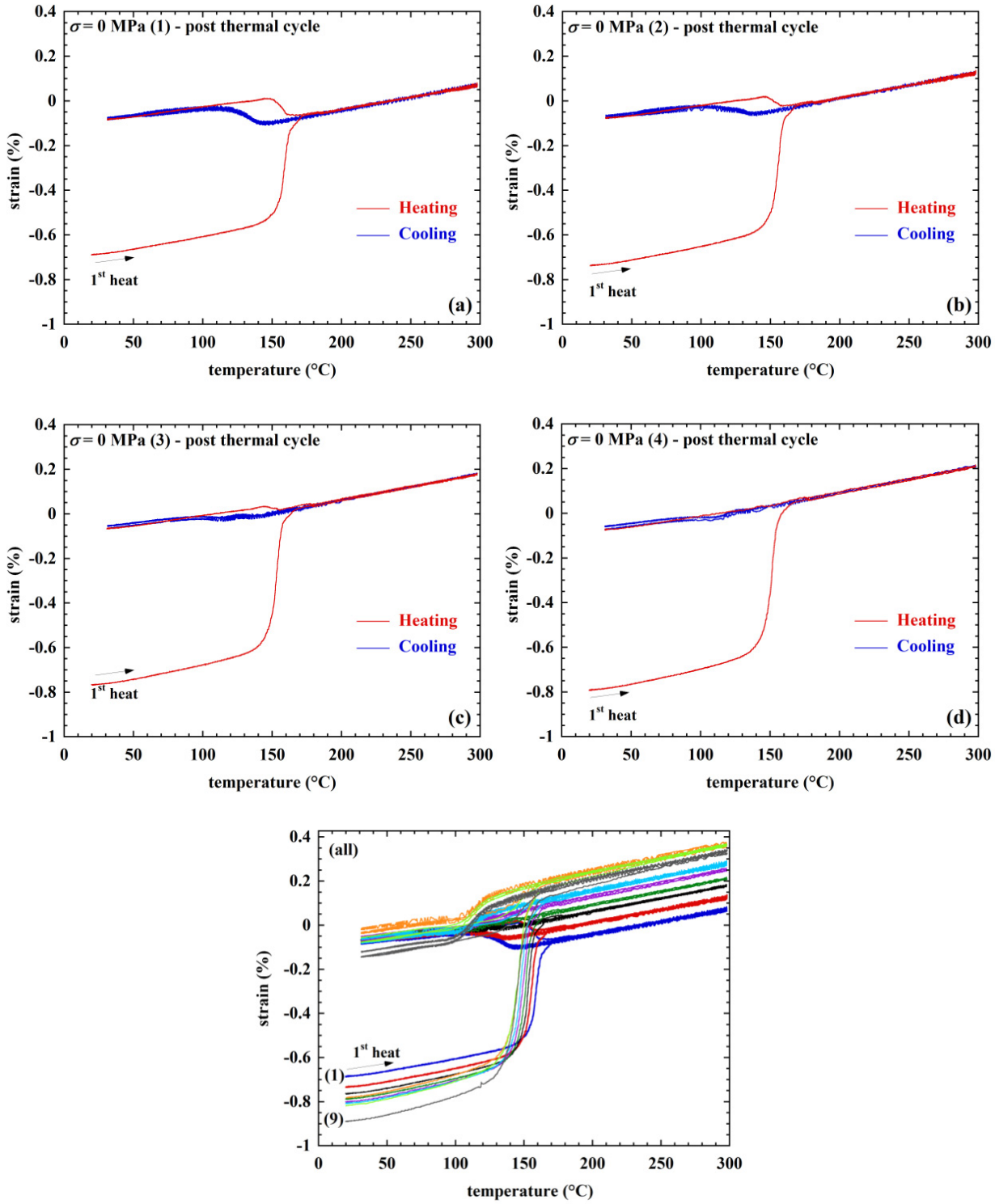

Figure 16.—Strain–temperature responses of the $Ni_{50.3}Ti_{29.7}Hf_{20}$ at 0 MPa stress. Each two cycles were performed subsequent to the constant strain, thermal cycling. For comparison purposes, all responses were plotted in the middle figure, while the individual responses are shown for sequences 1 to 8 labeled on the upper right corner of each plot.

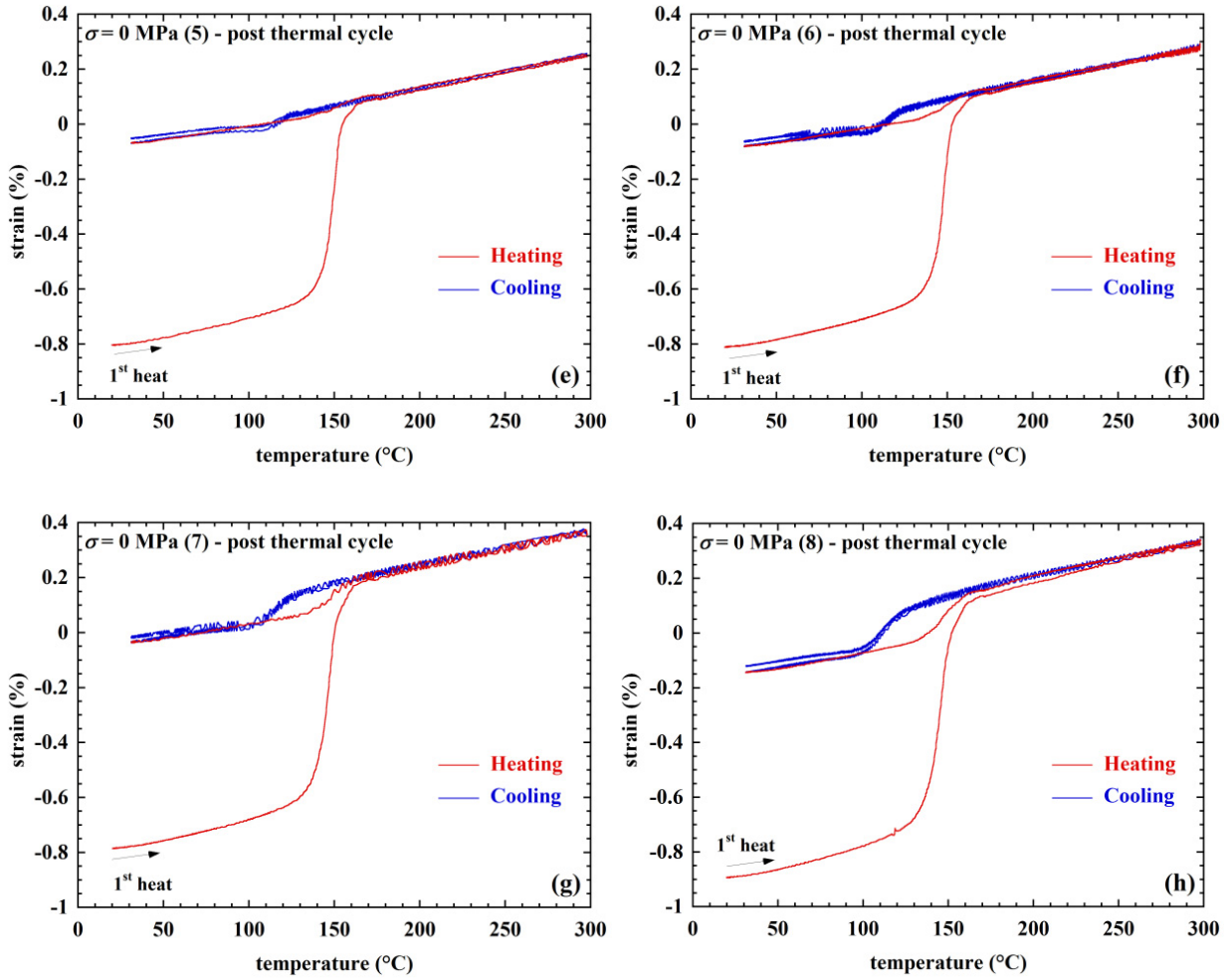

Figure 16.—Concluded.

Figure 17.—SMARS prototype testbed and enclosure with temperature controller. (b) Prototype kit of several SMAs with different end-conditions, heaters, and resetting platens.

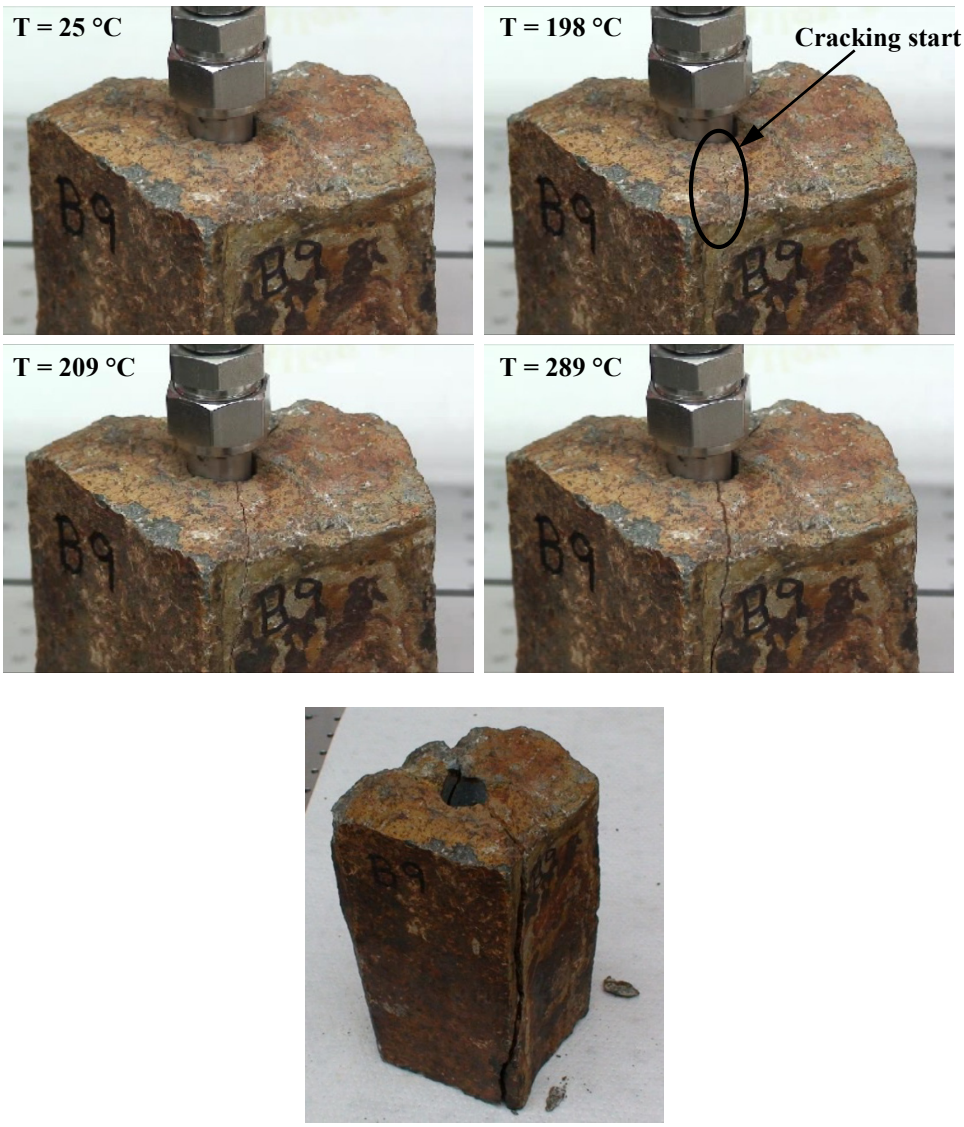

Figure 18.—Basalt test with $Ni_{50.3}Ti_{29.7}Hf_{20}$ trained using the isobaric method under –200 MPa. The sample was placed ~2.5 in. deep within the borehole.

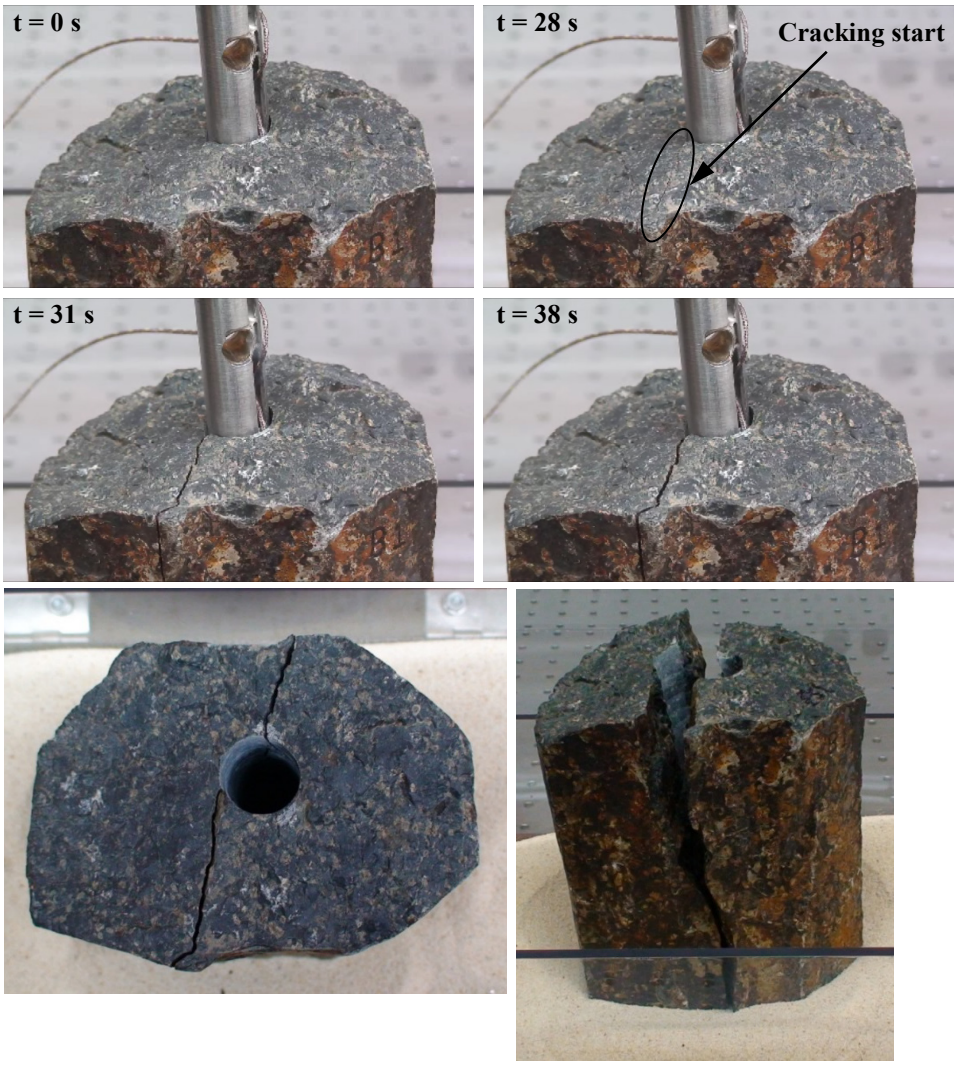

Figure 19.—Basalt test with $Ni_{49.9}Ti_{50.1}$ trained using the isobaric method under –300 MPa. The sample was placed ~0.5 in. deep within the borehole.

Granite rocks were tested using $Ni_{50.3}Ti_{29.7}Hf_{20}$ samples trained using the isobaric method under –300 MPa (Figure 20) and the isothermal method to –1 GPa followed by unloading to zero stress (Figure 21). In the first example, the isobarically trained SMA element was placed 2.5 in. deep within the borehole and resulted in a sudden and complete fracture of the rock sample. Similar to the basalt rocks, cracking was audible before the break, which took place at approximately 249 °C. In the second example, the isothermally trained SMA element was placed only 2.0 in. deep within the borehole and resulted in a more controlled cracking starting at 291 °C. Although the granite in this example did not fully split, this case serves to demonstrate a more controlled fracture process by regulating the SMA placement within the borehole.

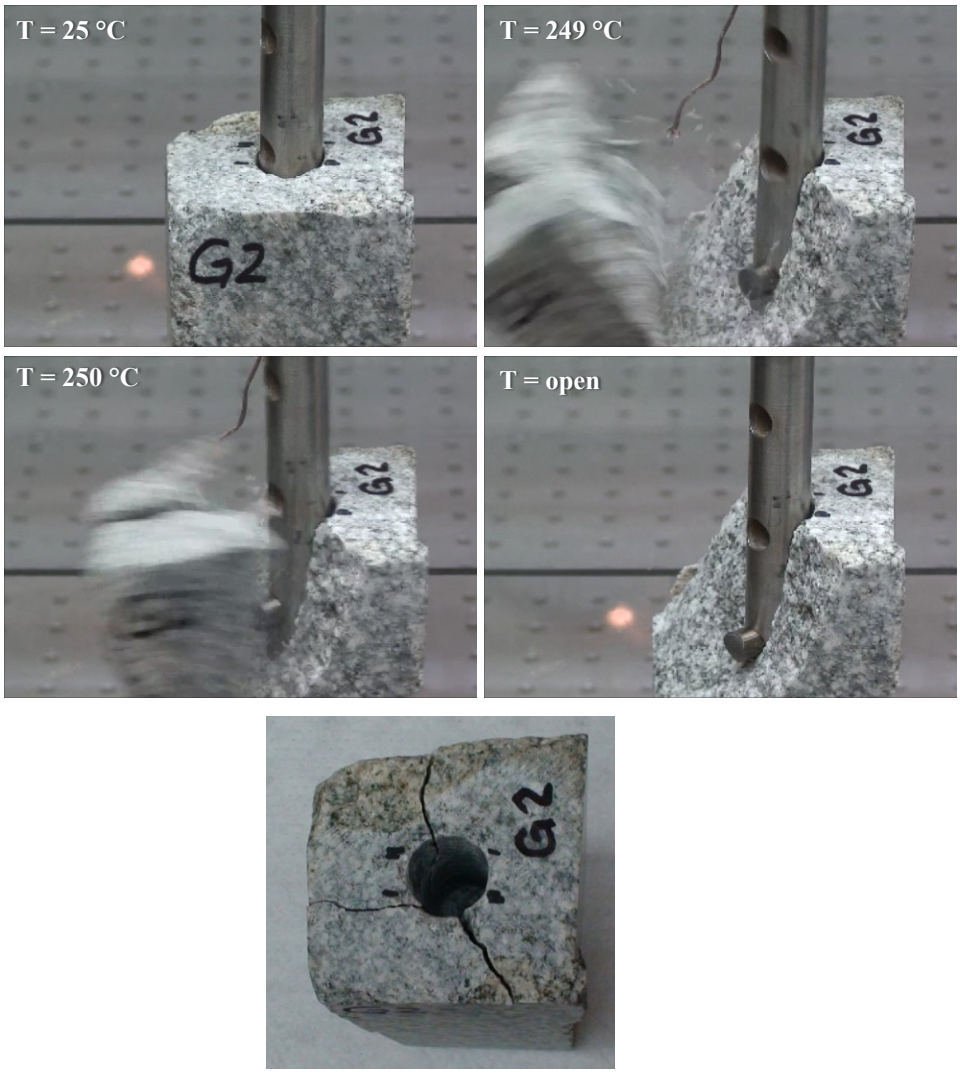

Figure 20.—Granite test with $Ni_{50.3}Ti_{29.7}Hf_{20}$ trained using the isobaric method under –300 MPa. The sample was placed ~2.5 in. deep within the borehole.

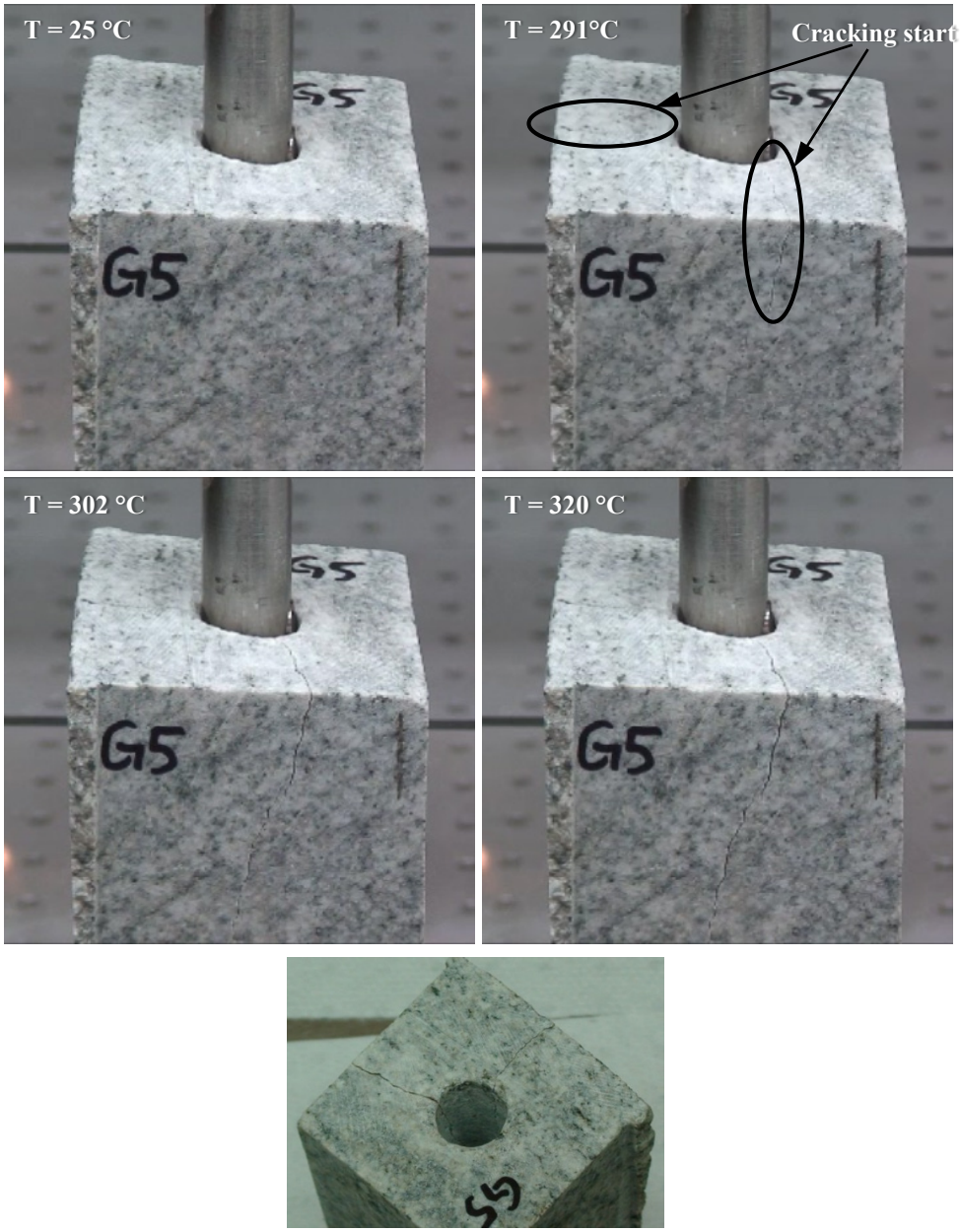

Figure 21.—Granite test with $Ni_{50.3}Ti_{29.7}Hf_{20}$ trained using the isothermal method to 1 GPa (followed by unloading). The sample was placed ~2 inches deep within the borehole.

Limestone (Figure 22) and sandstone (Figure 23) rock samples were tested using binary NiTi elements isobarically trained under –200 and –100 MPa. Due to the nature of the rocks, cracking was achieved in most cases but a small hand pressure was necessary to split the rocks in half. It was observed that these kind of rocks crumble at the SMA/rock contact area requiring more strain for a full fracture. The SMA pushers (Figure 4) were designed for this purpose where additional displacement is needed, at stresses beyond what you can do by hand.

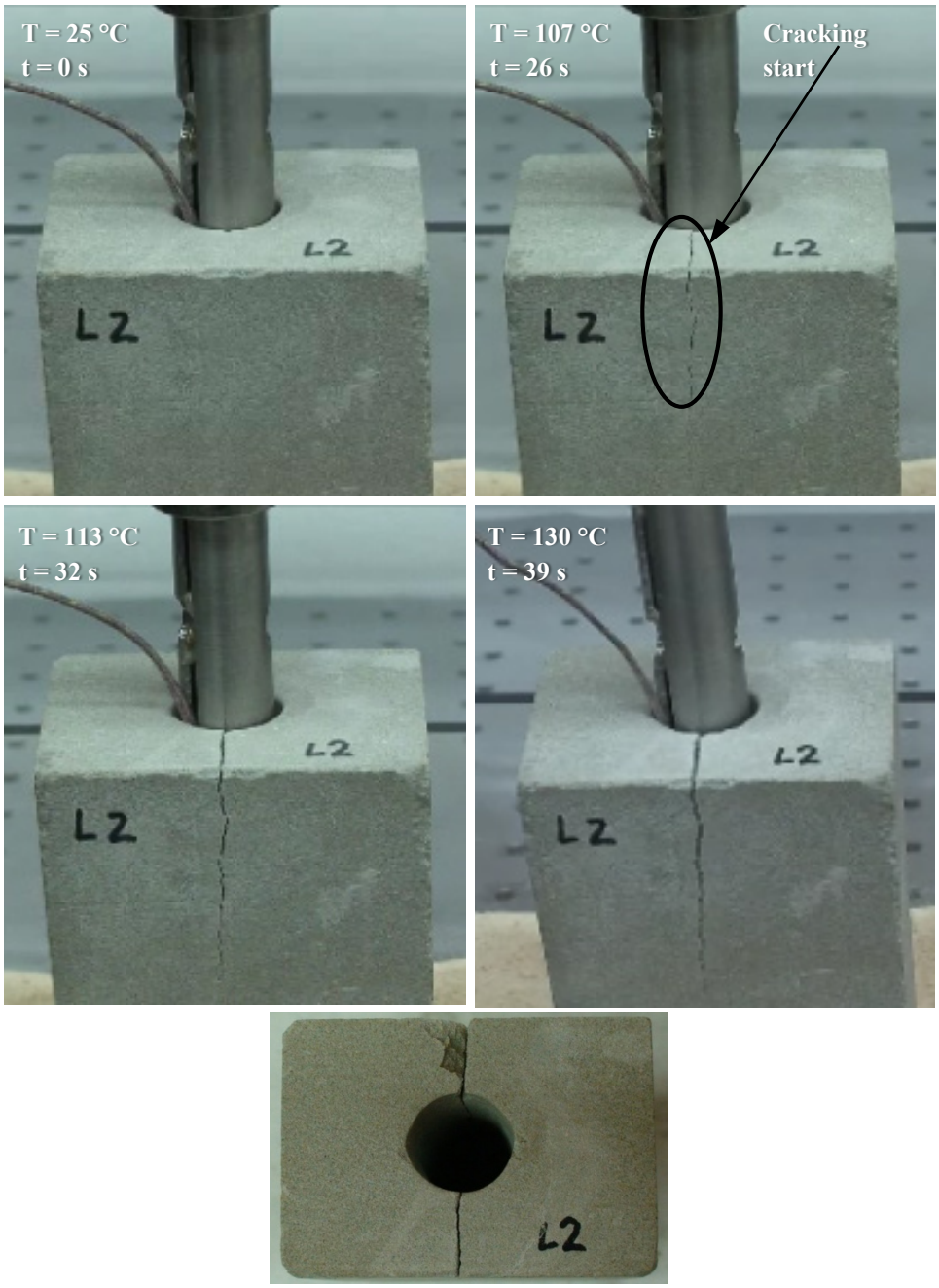

Figure 22.—Limestone test with $Ni_{49.9}Ti_{50.1}$ trained using the isobaric method under –200 MPa. The sample was placed ~0.75 inches deep within the borehole.

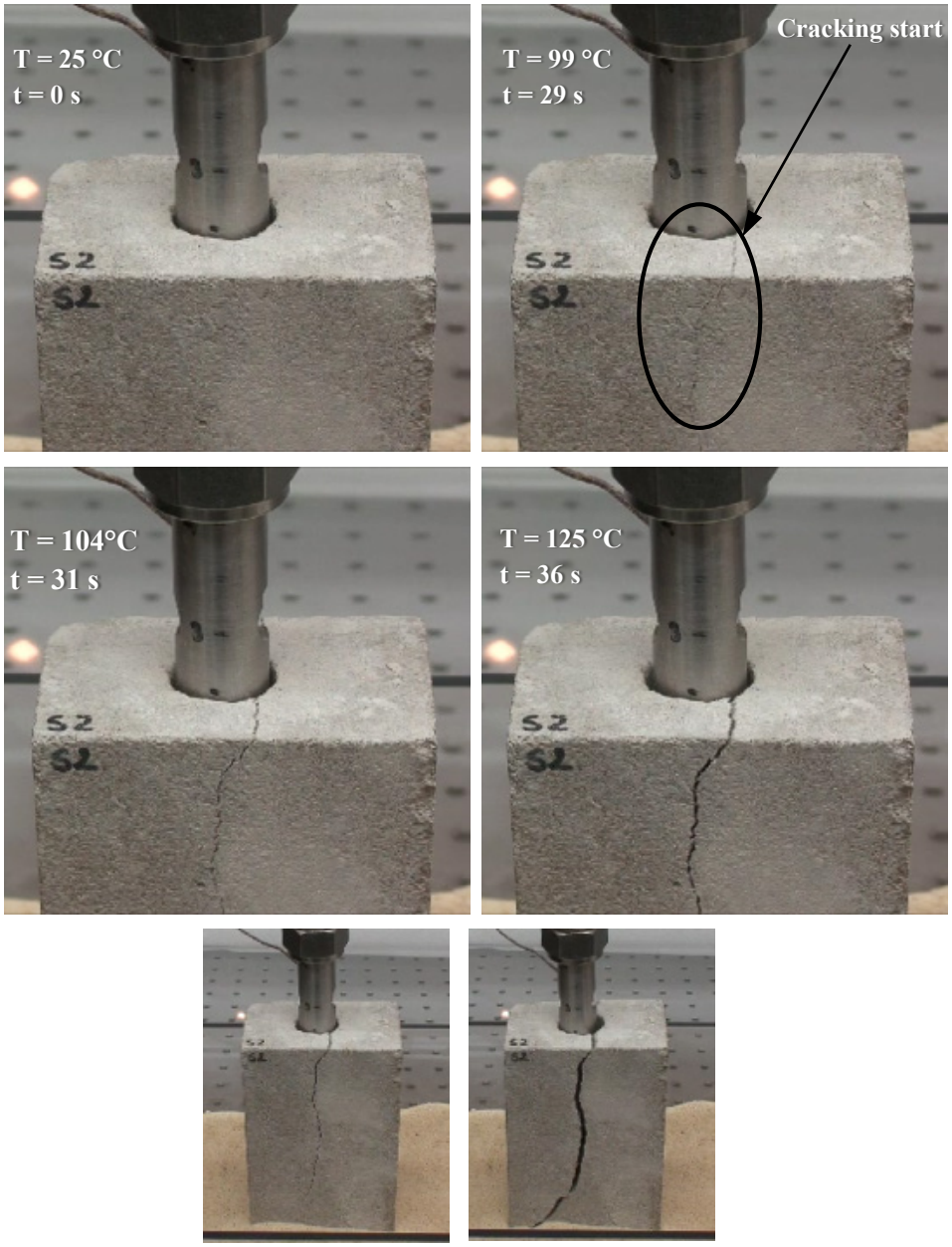

Figure 23.—Sandstone test with $Ni_{49.9}Ti_{50.1}$ trained using the isobaric method under –100 MPa. The sample was placed ~2.5 inches deep within the borehole.

7.0 Potential Applications

The SMARS device is targeted for static rock breaking, particularly when in situ extraction and analysis are imposed. It provides new solutions for sample extraction with significant reduction in weight, volume, and design complexity that would otherwise be deemed impractical for flight. The compactness and small footprint of the SMARS device makes it a possible candidate for future instrument packages onboard spacecraft and rovers (e.g., Mars missions, etc.). The application of SMARS is fast (seconds from activation to rock splitting), non-disturbing to the surrounding environments (e.g., no adverse vibration effects), and a clean process (no dust or flying debris). Analysis of rocks in planet Mars is one potential application for this device. SMARS enables the splitting of a rock or crater formation of interest

where in situ investigation is targeted. The inner structure of rocks that have not been exposed to the elements can hold clues to the past or presence of key minerals. It is envisioned that SMARS can be made part of an excavation tool comprised of drill heads, SMARS, and grippers (Figure 24). Another potential application is asteroid sampling as part of the NASA's Asteroid Redirect Mission (ARM). Once the asteroid mass is redirected to orbit the Moon, SMARS can be used (either by robots or astronauts) to break a piece of the asteroid and bring it back to planet Earth for detailed analyses. SMARS is advantageous in this case over other methods since gravitation forces are not required to activate the device. While rock splitting is the concept in hand, SMARS can also be used in non-rock related applications. For example, the concept can be used as a proppant or spacers to unjam a trapped component.

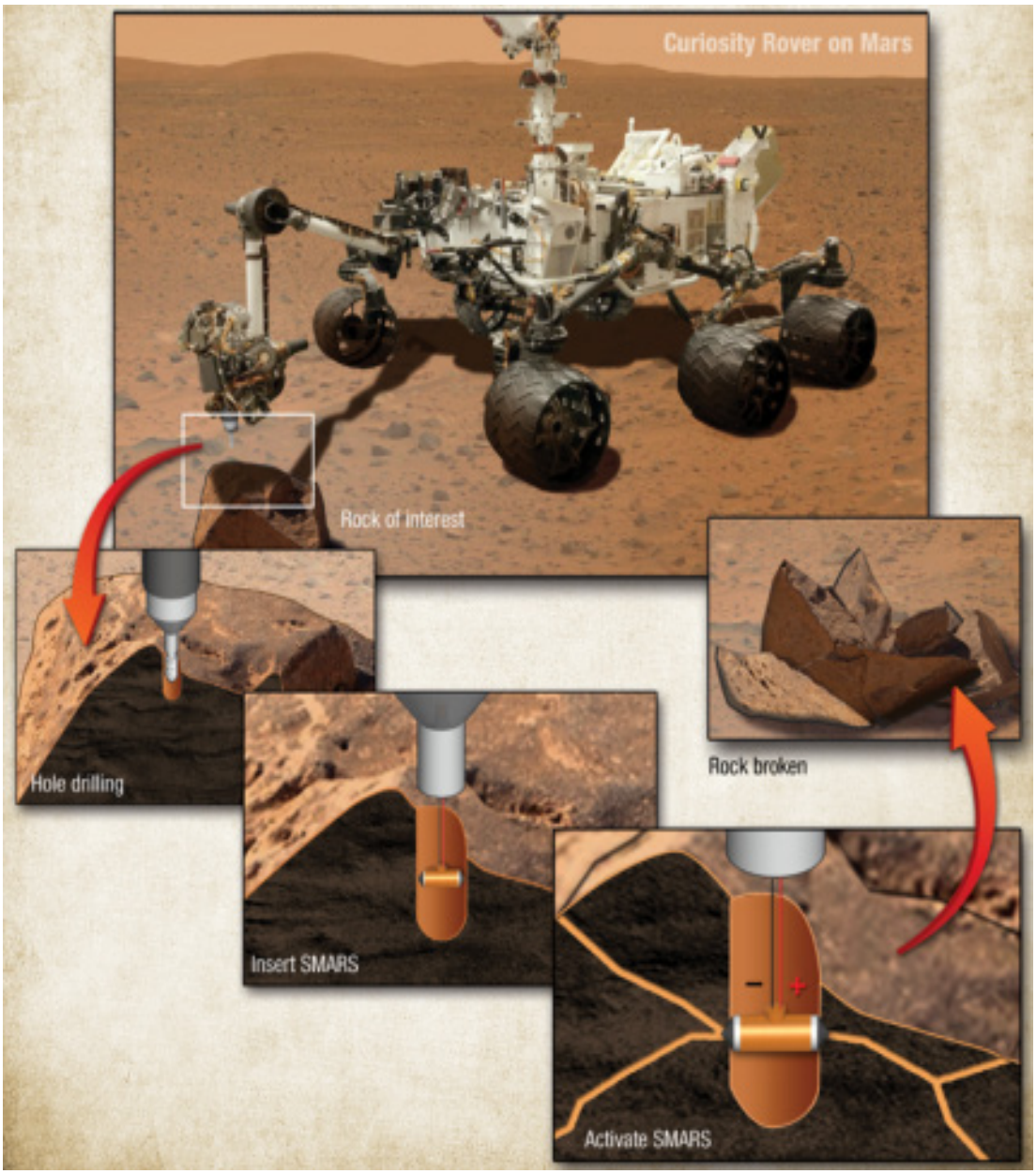

Figure 24.—Future prospects and applications of SMARS in space missions.

The SMARS device development can also be extended to the applicability of ground-based systems such as oil drilling, mining, fossil collecting and retrieval of other fragile geologic samples, proppants, civil engineering and other fields requiring compact but large static forces (Figure 25). It can also be used for structure reinforcement and corrective force applications to structural members and other engineering components.

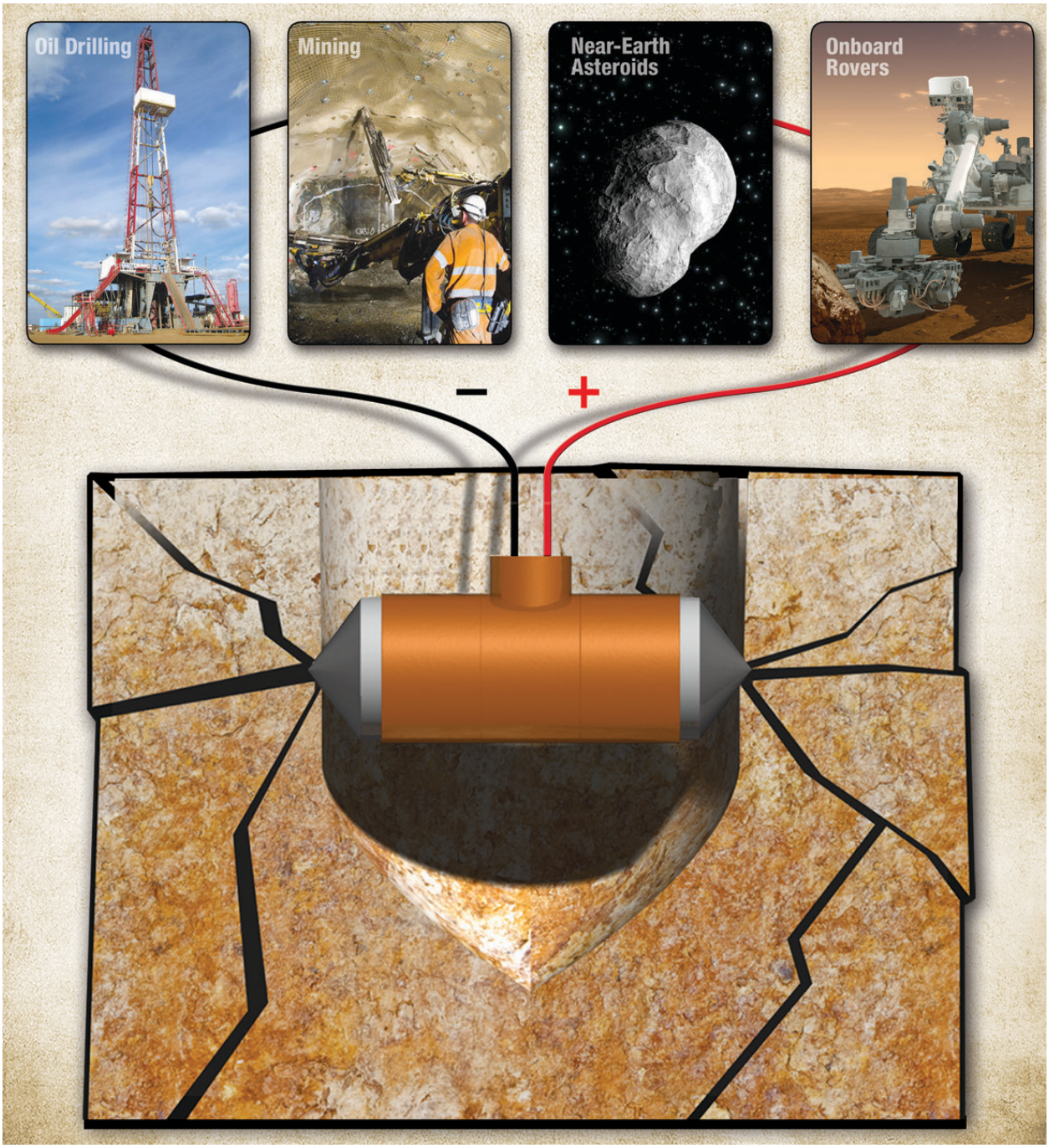

Figure 25.—Future prospects for SMARS in terrestrial applications.

8.0 Conclusions

A static shape memory alloy rock splitter (SMARS) along with supporting hardware including a custom heating system, detachable end-tips, and a modular controller was designed and tested using a precipitation strengthened, Ni-rich $Ni_{50.3}Ti_{29.7}Hf_{20}$ (at.%) alloy.. The device was built particularly for space-related applications where sampling geological deposits is required in extraterrestrial environments including planetary bodies such as the Moon, Mars, and near-Earth asteroids. The distinctive characteristics of this work are summarized below:

- The Ni-rich $Ni_{50.3}Ti_{29.7}Hf_{20}$ alloy exhibited inherently good force generation capability with activation temperature above 100 °C. This heat treatable, precipitation strengthened alloy was capable of generating stresses in excess of 1.5 GPa.
- Several training methods were used to maximize the force generation including isothermal and isobaric methods. Isobaric training was found to be the most efficient method and yielded the highest blocking stresses.
- Repeated cycling of the $Ni_{50.3}Ti_{29.7}Hf_{20}$ alloy elements indicated that recurrent use did not degrade the operability of the SMA elements and actually resulted in greater blocking stress capability with continued application.
- SMARS functionality was demonstrated on multiple rock types including igneous rocks (i.e., basalt, granite) and sedimentary rocks (i.e., sandstone, limestone), all of which were successful.

References

1. M. Nishida, K. Kaneko, T. Inaba, A. Hirata, K. Yamauchi, Static rock breaker using TiNi shape memory alloy, Materials Science Forum, 56 (1991) 711-716.
2. T. Inaba, M. Nishida, K. Kaneko, K. Yamauchi, Static Rock Breaker Using Shape Memory Alloy, in: 7th International Society for Rock Mechanics Congress, Aachen, Germany, 1991.
3. M. Nishida, K. Kaneko, K. Takashima, K. Yamauchi, T. Inaba, Practical Application of Static Rock Breaker Using TiNi Shape Memory Alloy, in: C.T. Liu, M. Wuttig, K. Otsuka, H. Kunsmann (Eds.) MRS Proceedings, vol. 246, 1991, pp. 415.
4. K. Yamauchi, T. Inaba, M. Nishida, K. Kaneko, Development of Static Rock Breaker Using TiNi Shape Memory Alloy as Pressure Source, Bulletin of the Japan Institute of Metals, 31 (1992) 550-552.
5. S. Carosio, P. Pozzolini, J. Van Humbeeck, G. Firstov, I. Sutherland, E. Tinnion, F. Jowitt, Application of Shape Memory Alloys to Develop a Massive Actuator for Rock Splitting, in: Pelton A.R., T. Duerig (Eds.) SMST 2003: Proceedings of the International Conference on Shape Memory and Superelastic Technologies, Pacific Grove, CA, 2003, pp. 629-637.
6. S. Carosio, D. Zangani, E. Parker, I. Sutherland, Application of Shape Memory Alloys to Rock Splitting: A Successful Example of Cooperation between Space Research and Industry, in: R.A. Harris, D. Raitt (Eds.) 2nd Conference on Academic and Industrial Cooperation in Space Research, ESA SP-470, Graz, Austria, 2000, pp. 27-32.
7. H. Jing, P. Shao, Z. Xu, H. Zhang, Y. Zhang, J. Zhou, Shape memory alloy stone breaker, CN201520012 (U), in, 2010.
8. P. Shao, H. Jing, Z. Xu, H. Zhang, Y. Zhang, J. Zhou, Device and method for directional fracture of rocks, CN101726223(B), in, 2013.
9. H. Jing, P. Shao, Z. Xu, H. Zhang, Y. Zhang, J. Zhou, Silent blast spalling device, CN201521303(U), in, Google Patents, 2010.

10. I.S. An, T.H. Nam, Static Stone Breaker Using Ternary Shape Memory Alloy of Ti-Ni-Cu, Patent: KR20010065983 (A), in, 2001.
11. S.S. Lee, Stress transfer device and method of a static rock crusher using wedge type expansive deformation of a shape memory alloy capable of crushing rock effectively by maximizing the displacement of deformation, Patent: KR2005075669 (A), in, 2005.
12. A. Glushchenkov Vladimir, P. Smelyakov Evgenij, N. Dunaev Aleksandr, S. Feoktistov Vasilij, A. Egorov Yurij, Apparatus for Breaking Monolithic Objects, Patent: SU1153061 (A1), in, 1985.
13. I.V. Chevakin, N.P. Zharov, O.V. Popov, A.I. Pesin, P.A. Radchenko, Power actuator, U.S. Patent 5,012,649, in, 1991.
14. K. Yamauchi, S. Sato, Shape Memory Alloy for Rock Crusher, Japanese Patent JPH04141562 in, 1992.
15. K. Watabe, Static Crushing Agent, Japanese Patent H04319181A, in, 1992.
16. J.G.C. Coenen, C.J. Kenter, D.H. Zijsling, Method and tool for fracturing an underground formation, U.S. Patent 6,176, 313, in, 2001.
17. J.J. Pelgrom, Method for placing a body of shape memory metal within a tube, U.S. Patent 5,040,283., in, 1991.
18. O. Benafan, R. Noebe, Shape Memory Alloy Rock Splitters (SMARS) – A Non-Explosive Method for Fracturing Planetary Rocklike Materials and Minerals, LEW-19195-1, March 03, 2014.
19. G. Firstov, J. Van Humbeeck, Y. Koval, High Temperature Shape Memory Alloys: Problems and Prospects, J. Intell. Mater. Syst. Struct., 17 (2006) 1041-1047.
20. T. Inaba, A. Hirata, K. Ishiyama, Rock Crushing Method, Japanese Patent JPH04108993A, in, 1992.
21. J.V. Booth, S.S. Sharples, Process for splitting granite, marble, and other rocks, US Patent 1,719,257, in, 1929.
22. I. Yoshishige, K. Yoshio, K. Masatada, Method of destroying ferroconcrete, rock or the like, US Patent 3,580,637, in, 1971.
23. A. Cerny, Splitting apparatus and method, U.S. Patent 4,740,036, in, 1988.
24. G.S. Pettifer, P.G. Fookes., A revision of the graphical method for assessing the excavatability of rock, Q. J. Eng. Geol. Hydroge., 27 (1994) 145-164.
25. C. Young, Controlled-foam injection for hard rock excavation, in: Proc. 37th U.S. Rock, Mechanics Symposium, Vail, CO, 1999.
26. W. Baum, Burners for flame jet drill, U.S. Patent 4,073,351, in, 1978.
27. H. Frankle, W. Baum, Flame jet tool for drilling cross-holes, US Patent 4,066,137, in, 1978.
28. H.Q. Van der Westhuizen, T.M. Muller, Barrel for rock breaking tool and method of use, U.S. Patent 4,900,092, in, 1990.
29. G.M. Wilkinson, Method and apparatus for plasma blasting, U.S. Patent 5,425,570, in, 1995.
30. S.P. Singh, Non-explosive applications of the PCF concept for underground excavation, Tunn. Undergr. Sp. Tech., 13 (1998) 305-311.
31. T. Caldwell, A comparison of non-explosive rock breaking techniques, in: School of Engineering, The University of Queensland, 2004.
32. J. Res, K. Wladzielczyk, A.K. Ghose, Environment-Friendly Techniques of Rock Breaking, CRC Press, 2003.
33. Rock Excavation Handbook, Matti Heiniö, Ed., Finland, Sweden: Sandvik Tamrock Corp., 1999.
34. P.N. Worsey, I.W. Farmer, G.D. Matheson, The Mechanics of Pre-Splitting In Discontinuous Rock, in, American Rock Mechanics Association, 1981.
35. G.P. Fauquier, Trim Blasting and Double Benching for Steeper Slopes and Competent Walls at PMC, Eng. Min. J., 184 (1983) 46-52.

36. Zhang Zhi-cheng, Chuan-jin Pu, Jin-jin Shi, Rock Damnification by Smooth Blasting of Different Charge Structures [J], Blasting, 1 (2006) 010.
37. O. Benafan, A. Garg, R.D. Noebe, G.S. Bigelow, S.A. Padula II, D.J. Gaydosh, N. Schell, J.H. Mabe, R. Vaidyanathan, Mechanical and functional behavior of a Ni-rich $Ni_{50.3}Ti_{29.7}Hf_{20}$ high temperature shape memory alloy, Intermetallics, 50 (2014) 94-107.
38. O. Benafan, R.D. Noebe, S.A. Padula II, R. Vaidyanathan, Microstructural Response During Isothermal and Isobaric Loading of a Precipitation-Strengthened Ni-29.7Ti-20Hf High-Temperature Shape Memory Alloy, Metall. Mater. Trans. A, 43A (2012) 4539-4552.
39. D.J. Hartl, D.C. Lagoudas, Aerospace applications of shape memory alloys, Proceedings of the Institution of Mechanical Engineers, Part G: Journal of Aerospace Engineering, 221 (2007) 535-552.
40. S.A. Padula II, Thermomechanical methodology for stabilizing shape memory alloy (SMA) response, US 8,409,372 B1, in, 2013.
41. S.A. Smith, E.D. Hodgson, Shape Setting Nitinol, in: S. Shrivastava (Ed.) Materials and Processes for Medical Devices Conference, Anaheim, CA, 2004, pp. 266-270.
42. O. Benafan, S.A. Padula II, R.D. Noebe, T.A. Sisneros, R. Vaidyanathan, Role of B19' martensite deformation in stabilizing two-way shape memory behavior in NiTi, J. Appl. Phys., 112 (2012) 093510.
43. O. Benafan, S.A. Padula II, R.D. Noebe, D.W. Brown, B. Clausen, R. Vaidyanathan, An in situ neutron diffraction study of shape setting shape memory NiTi, Acta Mater., 61 (2013) 3585-3599.
44. D.R. Coughlin, P.J. Phillips, G.S. Bigelow, A. Garg, R.D. Noebe, M.J. Mills, Characterization of the microstructure and mechanical properties of a 50.3Ni–29.7Ti–20Hf shape memory alloy, Scr. Mater., 67 (2012) 112-115.